Fall 2007

New techniques to improve power quality and evaluate stability in modern all-electric naval ship power systems

Peng Xiao

Department: Electrical and Computer Engineering

NEW TECHNIQUES TO IMPROVE POWER QUALITY AND EVALUATE STABILITY IN MODERN ALL-ELECTRIC NAVAL SHIP POWER SYSTEMS

by

PENG XIAO

A DISSERTATION

Presented to the Faculty of the Graduate School of the

UNIVERSITY OF MISSOURI-ROLLA

In Partial Fulfillment of the Requirements for the Degree

DOCTOR OF PHILOSOPHY

in

ELECTRICAL ENGINEERING

2007

Approved by

Keith A. Corzine, Co-advisor	Ganesh K. Venayagamoorthy, Co-advisor
Mehdi Ferdowsi	Badrul Chowdhury

Daniel S. Stutts

PUBLICATION DISSERTATION OPTION

This dissertation consists of the following three articles that have been submitted for publication as follows:

Pages 5-26 have been submitted to IET ELECTRIC POWER APPLICATIONS.

Pages 27-66 have been submitted to IEEE TRANSACTIONS ON POWER ELECTRONICS.

Pages 67-90 have been submitted to IEEE TRANSACTIONS ON POWER ELECTRONICS.

ABSTRACT

This dissertation focuses on two crucial issues in the design and analysis of the power electronic systems on modern all-electric naval ships, i.e., power quality control and stability evaluation. It includes three papers that deal with active power filter topology, active rectifier control, and impedance measurement techniques, respectively.

To mitigate harmonic currents generated by high-power high-voltage shipboard loads such as propulsion motor drives, the first paper proposes a novel seven-level shunt active power filter topology, which utilizes tapped reactors for parallel operations of switching devices. The multi-level system has been implemented in both regular digital simulation and real-time digital simulator for validation.

In the second paper, a harmonic compensation algorithm for three-phase active rectifiers is proposed. Based on the theory of multiple reference frames, it provides fast and accurate regulation of selected harmonic currents so that the rectifier draws balanced and sinusoidal currents from the source, even when the input voltages are unbalanced and contain harmonics. Extensive laboratory tests on a 2 kW prototype system verifies the effectiveness of the proposed control scheme.

The last paper presents a new technique for impedance identification of dc and ac power electronic systems, which significantly simplifies the procedure for stability analysis. Recurrent neural networks are used to build dynamic models of the system based on a few signal injections, then the impedance information can be extracted using off-line training and identification algorithms. Both digital simulation and hardware tests were used to validate the technique.

ACKNOWLEDGMENTS

First of all, I would like to express my sincere gratitude to Dr. Keith Corzine, my advisor and mentor, for his enthusiastic support and guidance along the years. I am truly grateful that he provided me with rewarding research opportunities and valuable experience in the areas of power electronics and motor drives. He continually stimulated my analytical thinking and greatly assisted me with technical writing.

Major thanks to my co-advisor Dr. Ganesh Venayagamoorthy, who encouraged me to explore the areas of computational intelligence. This work would not have been realized without the technical expertise and tireless support from him.

I am very grateful for having an exceptional doctoral committee and wish to thank Dr. Mehdi Ferdowsi, Dr. Badrul Chowdhury, and Dr. Daniel Stutts for their generous time and commitment. Their energetic, timely efforts and feedback were critical to my doctoral study and the completion of this work.

I am also indebted to my fellow colleagues, Dr. Yakov Familiant, Dr. Shuai Lu, Bojan Djokanovic, and Jerry Tichenor, for their academic support and cooperation over the years. Their help and friendships have made a difference in my research and life.

I wish to thank my dear parents and in-laws for their ever-willing assistance and love. Thanks are also due to my son, James, for the great joy he brings to our family.

Above all there is one person without whom all my efforts would have been in vain. My very special thanks to my wife, Jing Huang, who has been the backbone of my family and shouldered far more than half of the responsibilities. She's provided me not only her love but also the demonstration of it in the vital support and encouragements I needed, when I've most needed them.

Finally, I would like to gratefully acknowledge support for this work from the National Science Foundation, the Office of Naval Research, and the Naval Surface Warfare Center.

TABLE OF CONTENTS

LIST OF ILLUSTRATIONS

LIST OF TABLES

INTRODUCTION

In modern naval shipboard power systems, high power density semiconductor devices and compact high power drives have enabled the use of Integrated Power System (IPS) architecture which can provide high system reliability, increased survivability, and sufficient redundancy. The developments in power electronic devices and their integration at all levels in the power system not only provide exceptional performance gain and enormous operational flexibility, they also pose great challenges.

In this dissertation, two crucial issues in the design and analysis of shipboard power systems are discussed. The first issue is power quality, which is an especially important aspect of naval power applications due to the requirement for low detectability. The stability of the system is the other issue. With multiple loads connected to the dc link in a dc zonal distribution system, the design and analysis of the power system has become a major issue due to increased dynamics and probable instability. The constant power operation capability of most power electronic converters often leads to negative impedance characteristic, which is a common cause for system instability.

Poor power quality can be caused by a variety of factors. However, high-power nonlinear loads such as diode/SCR rectifiers for propulsion motor drives are the major sources of harmonic currents. Such power converters have low switching frequency and generate large amount of low-order harmonic currents. When these distorted currents flow through the power system, they would cause distortions in bus voltages, which in turn may affect the normal operation other non-polluting loads in the same system.

Two approaches are considered in this work to address the issue of power quality. In the first paper, harmonic compensation devices are used to reduce the harmonic

currents generated by nonlinear loads. Specifically, a seven-level shunt active power filter topology is proposed to inject into the system the same amount of harmonic currents the nonlinear loads need, thus eliminating their impacts on other part of the system. The use of a seven-level converter serves three purposes. Firstly, it reduces voltage stress across the switching devices by using series-connected devices in a flying capacitor structure. Secondly, it reduces the current rating requirements on the switching devices by distributing the compensation currents between two parallel three-level converters. Finally, multi-level converter provides much lower total harmonic distortion in terms of low-order harmonics generated by pulse width modulation. Extra benefits of the proposed topology also include lower dv/dt and smaller passive filter requirement. The detailed model of the topology and control algorithms are described in Paper I. In addition, a joint redundant state selection (JRSS) algorithm is adopted to balance the voltages applied across the tapped reactors so that the magnetizing currents are minimized. To validate the proposed topology and control schemes, an example shipboard power system was implemented in both a regular digital simulator and a Real-Time Digital Simulator (RTDS). Good agreements were achieved between the results of the two environments.

Although improving the overall power quality of the shipboard power system can be accomplished by compensation at the source of power pollution, each power component should also have the ability to handle a certain amount of distortions in the system. This is especially critical for naval ships because of the possibilities of battle damage and disruptions during operation. This aspect of the power quality issue is addressed in the second paper, where a novel multiple reference frame (MRF) based harmonic compensation algorithm is proposed for the control of three-phase active

rectifiers under unbalanced and harmonic input voltage conditions. Conventional PWM rectifier controllers have limited bandwidth, which makes it very difficult to suppress the perturbations caused by distortions in the input voltages. In addition, non-ideal input conditions can degrade the performance of the controller and cause ripple in the output dc voltage. The proposed compensation algorithm targets a selected group of harmonic components in the input currents, and can achieve almost zero steady-state error for those harmonics. The use of a novel multiple reference frame scheme makes it possible to regulate the harmonic currents in a fast and accurate fashion. Based on the same MRF principle, a decoupled phase-locked loop algorithm is set forth in Paper II to precisely track the frequency and phase angle of the power system, which is an important issue for harmonic current compensation.

Stability analysis and evaluation is a fundamental task in the design and integration of large power electronic systems. In many cases, it is often necessary to obtain the frequency-dependent impedances or admittances of a subsystem by experimentation. Several impedance extraction techniques for dc and ac systems have been proposed in recent years. To get the frequency-dependent characteristics by experimentation, periodic voltage or current perturbations are usually injected to the system while it is under operational power. However, conventional impedance measurement process is often very time-consuming, and requires that the system is in operation at a fixed operating point for a long period of time because multiple injections are needed.

In the third paper included in this dissertation, a novel impedance identification method is proposed. Instead of injecting perturbation signals to the system one frequency

at a time, a randomized injection signal is employed, thus only a few set of the voltage and current measurements is required. The captured signals are then used to train a recurrent neural network (RNN) in an off-line mode. Once the RNN is trained, it approximates the dynamic behavior of the system in the time domain, and can also generalize the system responses in the frequency domain. Perturbation signals of different frequencies are then fed into the trained RNN to determine its frequency responses, which are very close to those of the tested system, as demonstrated by simulation and experimental results.

PAPER I

Seven-Level Shunt Active Power Filter for High Power Drive Systems

Peng Xiao, Ganesh K. Venayagamoorthy, and Keith A. Corzine

Real-Time Power and Intelligent Systems Laboratory

Department of Electrical and Computer Engineering

University of Missouri-Rolla, Rolla, MO, 65401 USA

pxfx7@umr.edu, gkumar@ieee.org and keith@corzine.net

ABSTRACT

In high-power adjustable speed motor drives, such as those used in electric ship propulsion systems, active filters provide a viable solution to mitigating harmonic related issues caused by diode or thyristor rectifier front-ends. To handle the large compensation currents and provide better thermal management, two or more paralleled semiconductor switching devices are often used. In this paper, a novel topology is proposed where two active filter inverters are connected with tapped reactors to share the compensation currents. The proposed active filter topology can also produce seven voltage levels, which significantly reduces the switching current ripple and the size of ripple filters. Based on the joint redundant state selection strategy, a current-balancing algorithm is proposed to keep the reactor magnetizing current to a minimum. It is shown through simulation that the proposed active filter can achieve high overall system performance. The system is also implemented on a real-time digital simulator to further verify its effectiveness.

Keywords

active power filter, multi-level converter, harmonic compensation

1. INTRODUCTION

Adjustable speed motor drives (ASDs) have found extensive application in a variety of high-power systems. One example is the electric propulsion system used in modern naval ships, the power ratings of which can be tens of megawatts. Typically the front-ends of such ASDs employ a diode or thyristor rectifier. In spite of their simple control and robust operation, these devices can result in serious power quality issues. They can generate voltage and current harmonics that might affect the operation of other devices in the same ac system. Conventionally, passive *L*-*C* filters are used to mitigate harmonic related problems. However, due to their large size and inflexibility, passive filters are gradually being replaced by active filters that utilize power electronic inverters to provide compensation for harmonics [1].

Among various active filter configurations, the shunt active filter systems have a number of advantages and constitute the optimal harmonic filtering solution for ASD rectifier front-ends [2]. In general, the ratings of shunt active filters are based on the rms compensating current and the rms filter terminal voltage. For high-power applications such as ship propulsion systems, the large compensation current often requires parallel operation of two or more switching devices or active filters.

In recent years, multilevel converters have shown some significant advantages over traditional two-level converters [2-3], especially for high power and high voltage applications. In addition to their superior output voltage quality, they can also reduce voltage stress across switching devices. Since the output voltages have multiple levels,

lower dv/dt is achieved, which greatly alleviates electromagnetic interference problems due to high frequency switching. Over the years most research work has focused on converters with three to five voltage levels [4-5], although topologies with very high number of voltage levels were also proposed [6]. In general, the more voltage levels a converter has the less harmonic and better power quality it provides. However, the increase in converter complexity and number of switching devices is a major concern for multilevel converter. It has been shown that although more voltage levels generally mean lower total harmonic distortion (THD), the gain in THD is marginal for converters with more than seven levels [7].

This paper presents a shunt active filter configuration that uses tapped reactors for harmonic current sharing. It reduces current stress of the switching devices by distributing the compensation current between two parallel legs of an H-bridge topology. It also reduces voltage stress across the switches by utilizing a conventional three-level flying capacitor topology. Overall, the configuration is capable of producing seven distinct voltage levels and thus greatly reduces switching ripple in the compensating currents.

The rest of this paper is organized as follows. The active filter topology is briefly described in Section 2. In Section 3, the operation of the tapped reactor is modeled in detail to illustrate its capability of generating multiple voltage levels. The control algorithm of the active filter is discussed in Section 4. To minimize the magnetizing currents in the reactors, a balancing algorithm based on the joint redundant state selection is presented which is discussed in Section 5. Simulation results are presented in Section 6 to evaluate the proposed configuration and control. In addition, the system is

implemented on a real-time digital simulator to further validate the proposed active filter, and the results are also presented in Section 6. Finally, the conclusions are given in Section 7.

2. ACTIVE FILTER TOPOLOGY

The *a*-phase of the proposed active filter topology is shown in Fig. 1. It consists of an H-bridge configuration made from three-level flying capacitor branches. Essentially, it is a voltage-source-inverter (VSI) with capacitive energy storage ($C_{\rm dc}$) shared by all three phases. A total of eight switching devices are used in each phase. A tapped reactor is used to connect the two legs of the H-bridge, and the output terminal is at the one-third tap of the reactor.

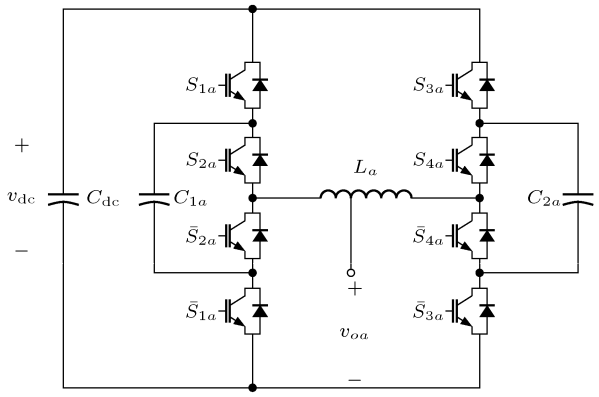

Fig. 1. Phase *a* of the seven-level active filter topology.

3. TAPPED REACTOR MODEL

Unlike the center-tapped inter-phase reactor used in [8-11], the reactor in the proposed topology has a tap terminal at its one-third position, as shown in Fig. 2. For the convenience of analysis, the reactor can be divided into two parts. In Fig. 2a, part one,

denoted as L_1, consists of the portion from terminal 1 to the tap and has a number of turns $N_1 = N$; part two, denoted as L_2, consists of the portion from the tap to terminal 2 and has a number of turns $N_2 = 2N$. Terminals 1 and 2 are defined as the input terminals while the tap terminal is defined as the output terminal, O.

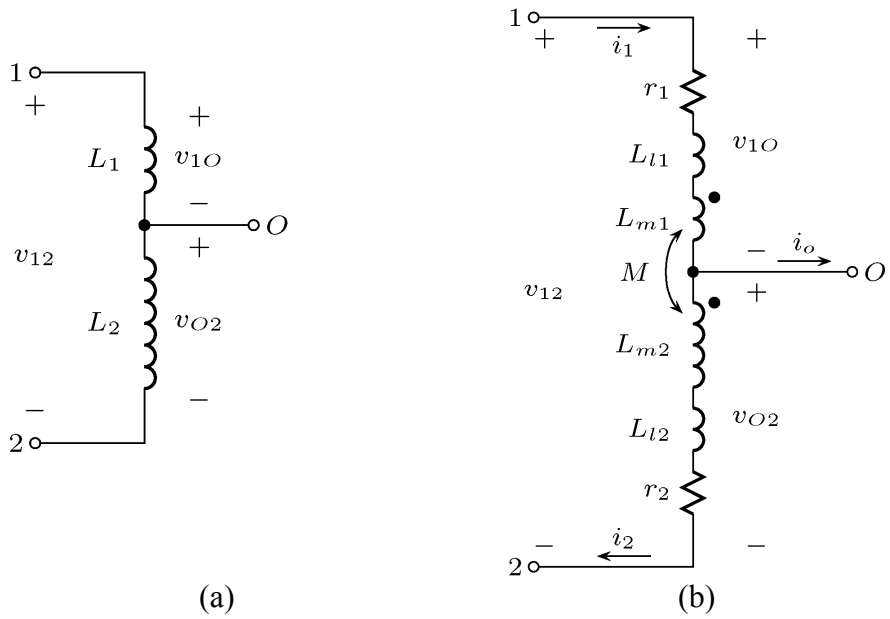

Fig. 2. Models of the tapped reactor: (a) ideal; (b) detailed.

3.1 Analysis of an Ideal Tapped Reactor

To derive the relationship between the input voltages and the output voltage, an ideal model of the tapped reactor is considered first in which there are no losses and no leakage flux. The following assumptions are made:

- The core of the reactor is highly permeable in a sense that it requires vanishingly small magnetomotive force to set up the flux.
- The core does not exhibit any eddy current or hysteresis loss.
- All the flux is confined in the core so there is no leakage flux.

- The resistance of the reactor is negligible.

Suppose that voltages v_1 and v_2, with respect to a common ground, are applied to the input terminals 1 and 2, respectively. The voltage across the two input terminals is denoted as $v_{12} = v_1 - v_2$. For this ideal model it is straightforward to determine the voltage between the output terminal O and terminal 2:

$$v_{O2} = \frac{N_2}{N_1 + N_2} v_{12} = \frac{2}{3}(v_1 - v_2). \quad (1)$$

The voltage at the output terminal with respect to the common ground is thus

$$v_O = v_{O2} + v_2 = \frac{2}{3} v_1 + \frac{1}{3} v_2. \quad (2)$$

Each leg of the H-bridge has a voltage-clamping capacitor and the voltages at the two input terminals of the reactor can be 0, $v_{dc}/2$, or v_{dc}, where v_{dc} is the nominal voltage of the capacitor C_{dc}. For each phase there are nine different switching states, corresponding to nine terminal voltage combinations (v_1, v_2). These combinations can produce a line-to-ground voltage v_O at the output terminal that has seven distinct voltage levels, as shown in Table I.

Table I. Voltage Relationship for Tapped Reactors.

State	v_1	v_2	v_O
0	0	0	0
1	0	$v_{dc}/2$	$v_{dc}/6$
2	$v_{dc}/2$	0	$v_{dc}/3$
2'	0	v_{dc}	$v_{dc}/3$
3	$v_{dc}/2$	$v_{dc}/2$	$v_{dc}/2$
4	$v_{dc}/2$	v_{dc}	$2v_{dc}/3$
4'	v_{dc}	0	$2v_{dc}/3$
5	v_{dc}	$v_{dc}/2$	$5v_{dc}/6$
6	v_{dc}	v_{dc}	v_{dc}

Note that there are two redundant states 2' and 4' that produce the same voltage as states 2 and 4, respectively. However, these are not desirable because the voltages applied across the reactor are twice as high as the other states.. The output current is shared by the two legs of the H-bridge, with one having one-third of the current and the other having two-thirds. Therefore, the switching devices can be rated at either one-third or two-thirds of the required compensating current level, depending on the reactor terminal these are connected to.

3.2 Non-ideal Reactor Model Analysis

The ideal reactor model demonstrates that with three-voltage levels at the input terminals, the output voltage can have seven distinct levels. In practice, winding resistance, leakage inductance, and magnetizing inductance should be taken into account to obtain more accurate voltage and current relationships for the purpose of analysis and simulation.

As shown in Fig. 2b, the detailed reactor model consists of two inductors that are coupled via a common core. The following quantities are defined:

- N_1, N_2: number of turns of each inductor, $N_1 = N$, $N_2 = 2N$
- r_1, r_2: winding resistance
- L_{l1}, L_{l2}: leakage inductance
- L_{m1}, L_{m2}: self inductances
- M: mutual inductance between the two inductors

For simplification, it is reasonable to assume that the winding resistance and leakage inductance of an inductor are proportional to its number of turns. Hence,

$$\begin{aligned} r_1 &= r \qquad r_2 = 2r \\ L_{l1} &= L_l \qquad L_{l2} = 2L_l \end{aligned} . \tag{3}$$

It can be shown that the relationship between the self inductances and mutual inductance is

$$L_{m1} = \frac{M}{2} \qquad L_{m2} = 2M \ . \tag{4}$$

Let the current through inductor L_1 be i_1 and the current through L_2 be i_2, then the voltage across L_1 is

$$v_{O1} = L_l \frac{di_1}{dt} + \frac{M}{2}\frac{di_1}{dt} + M\frac{di_2}{dt} + ri_1 , \tag{5}$$

and the voltage across L_2 is

$$v_{O2} = 2L_l \frac{di_2}{dt} + 2M\frac{di_2}{dt} + M\frac{di_1}{dt} + 2ri_2 . \tag{6}$$

By Kirchhoff's voltage and current laws, (5) and (6) can be re-written as

$$\begin{aligned} v_{O1} &= \frac{1}{3}v_{12} + \frac{2}{3}L_l\frac{di_o}{dt} + \frac{2}{3}ri_o \\ v_{O2} &= \frac{2}{3}v_{12} - \frac{2}{3}L_l\frac{di_o}{dt} - \frac{2}{3}ri_o \end{aligned} . \tag{7}$$

If L_l and r are negligible one would obtain the same results as in (1). The derivatives of inductor currents can be determined as

$$\begin{aligned} \frac{di_1}{dt} &= -\frac{2}{3}\frac{-2L_l\frac{di_o}{dt} - 3M\frac{di_o}{dt} - v_{12} + ri_o + 3ri_2}{2L_l + 3M} \\ \frac{di_2}{dt} &= -\frac{1}{3}\frac{2L_l\frac{di_o}{dt} + 3M\frac{di_o}{dt} - 2v_{12} + 2ri_o + 6ri_2}{2L_l + 3M} \end{aligned} . \tag{8}$$

Equations (7) and (8) are used to build a detailed model of a tapped reactor for simulation. It should be noted that since the output terminal is always connected to

another inductor, the three currents i_1, i_2 and i_o are not independent and only two of them can be chosen as system states.

3.3 Active Filter Interface

As shown in Fig. 3, The active filter is connected to the power system via a three-phase inductor L_f. The filtering function is achieved by injecting a compensating harmonic current into the point of common coupling of the utility-load interface, which in this case is the secondary side of the rectifier load transformer. The reference harmonic currents are extracted from the load currents so that the sum of the load currents and the injection currents has a total harmonic distortion that meets the required specifications. The seven-level inverter can produce an output voltage that contains much less switching frequency ripple than a conventional two-level inverter; thus, the generated injection currents are smoother. In addition, the size of the switching frequency passive filter can be significantly reduced.

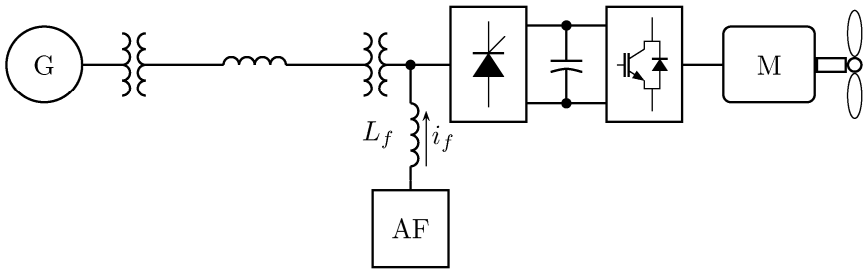

Fig. 3. Active filter connection to a shipboard power system.

4. ACTIVE FILTER CONTROL

To effectively compensate the load harmonic currents, the active filter controller should be designed to meet the following three goals:

- Extract and inject load harmonic currents
- Maintain a constant dc capacitor voltage
- Avoid generating or absorbing reactive power with fundamental frequency components

4.1 Harmonic Current Extraction

For diode or thyristor rectifier loads, the most common harmonic currents are of the 5^{th}, 7^{th}, 11^{th}, and 13^{th} order. Although a high-pass filter can be used to extract these components directly from the line currents, it is not feasible to obtain high attenuation at the fundamental frequency due to the high current amplitude. The synchronous *q*-*d* reference frame controller developed for shunt active filter systems is used to generate the reference compensating current [12]. As shown in Fig. 4, the load phase currents (i_{aL}, i_{bL}, and i_{cL}) are first transformed into the synchronous reference frame to obtain i_{qL} and i_{dL}. Low-pass filters are then used to extract the dc components, which correspond to the fundamental frequency components in the load currents. High-pass filters are implemented by removing the extracted dc components from i_{qL} and i_{dL}.

4.2 DC Capacitor Voltage Control

For the active filter to operate effectively it is important to maintain the dc capacitor voltage at a constant value. Since the active filter topology is essentially identical to that of an active rectifier, similar control strategies for the active rectifier are applicable.

The dc capacitor voltage is directly affected by the real power transferred across the active filter. To keep the voltage constant, ideally no real power should be transferred. However, due to losses in switching devices and other components, a small amount of

real power is needed. In the synchronous reference frame with the *q*-axis aligned with the voltage at the point of common coupling, the real power transferred can be expressed as

$$P = \frac{3}{2} v_{qs} i_{qf} , \tag{9}$$

which means that by adjusting the *q*-axis filter current the real power can be effectively controlled. The controller diagram is shown in Fig. 4.

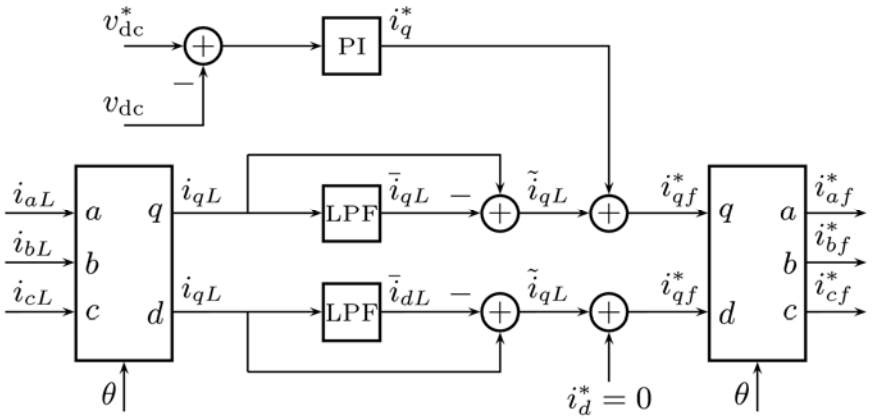

Fig. 4. Active filter control diagram.

4.3 Reactive Power Control

In most cases a unity power factor for fundamental frequency components is required at the active filter terminals. Since the reactive power can be expressed as

$$Q = \frac{3}{2} v_{qs} i_{df} , \tag{10}$$

This goal can be achieved by keeping the *d*-axis current at zero, as shown in Fig. 4. The combined control of dc capacitor voltage and reactive power uniquely determines the fundamental frequency component of the active filter output current. This

current is then superimposed onto the commanded harmonic currents, and the commanded filter currents i_{af}^{*}, i_{bf}^{*} and i_{cf}^{*} are obtained.

4.4 Harmonic Current Regulator

A current regulator is needed to generate the commanded compensation current. Generally, a hysteresis control provides fast response and is suitable for non-sinusoidal current tracking. However, it suffers from some serious disadvantages such as variable switching frequency and phase interaction problems [1]. In addition, to fully take advantage of the benefits of a multilevel converter, a current regulator that uses a voltage-source PWM modulation is desirable.

In this paper, a predictive current regulator is implemented to track the harmonic currents, which has the advantages of simple structure and less computational requirement. Given the system voltages and filter inductor currents, the required *a*-phase filter voltage can be calculated based on estimated values of the filter inductance

$$v_{af}^{*} = \hat{v}_{as} + \frac{(\hat{i}_{af}^{*} - i_{af})\hat{L}_{f}}{\Delta t}, \tag{11}$$

where Δt is the controller switching period, $\hat{v}_{as}$ is the predicted source voltage and can be calculated as

$$\hat{v}_{as} = v_{as}(t) + 1.5\Delta t[v_{as}(t) - v_{as}(t-\Delta t)], \tag{12}$$

and $\hat{i}_{af}^{*}$ is the predicted reference harmonic current

$$\hat{i}_{af}^{*} = i_{af}^{*}(t) + 2\Delta t[i_{af}^{*}(t) - i_{af}^{*}(t-\Delta t)]. \tag{13}$$

For accurate current tracking, the prediction takes into account the controller delay due to data acquisition and calculation. The active filter interface inductance L_f can be estimated online.

4.5 Multilevel Voltage Modulation

Once the commanded voltages v_{af}^*, v_{bf}^* and v_{cf}^* are calculated, the next step is to determine the switching signals that generate these voltages. The active filter can generate seven distinct voltage levels (0 to 6). The immediate levels below and above v_{af}^* can be determined by

$$ll_a = \text{int}(d_{am}) \qquad ul_a = ll_a + 1, \tag{14}$$

where the function int(.) truncates d_{am} to an integer and

$$d_{am} = \left(\frac{v_{af}^*}{V_{dc}} + 0.5 \right) \times 6 . \tag{15}$$

Note that ll_a should be limited in the range from 0 to 5.

To generate an average voltage of v_{af}^* in a switching period Δt, the active filter should generate voltage level ul_a for time duration t_a, and generate level ll_a for duration $\Delta t - t_a$. According to (14), d_{am} is a number between integers ll_a and ul_a, and $ul_a = ll_a + 1$. Thus,

$$d_{am} \times \Delta t = ll_a \times (\Delta t - t_a) + (ll_a + 1) \times t_a \tag{16}$$

The switching time is then calculated as

$$t_a = (d_{am} - ll_a) \Delta t . \tag{17}$$

To generate a specific output voltage level, Table I is first used to determine the voltage levels that should be applied to the reactor input terminals. Switching signals can then be determined for the two flying-capacitor converter legs to generate the required voltage levels.

5. MAGNETIZING CURRENT MINIMIZATION

5.1 Reactor Magnetizing Currents

The current through the reactor consists of two components. One is the compensating current that flows out of the tap terminal and is shared by the two parts of the reactor. The other is the magnetizing current that is generated when a dc voltage is applied across the reactor input terminals. The magnetizing current does not contribute to the filtering function and should be minimized to reduce current ratings of the switching devices and to avoid reactor saturation. Ideally, the magnetizing current has a zero dc component. In practice, however, the dc current tends to drift away from zero if uncontrolled because of the differences in component parameters and controller errors. Therefore, it is necessary to monitor and control the magnetizing currents of the three-phase reactor so that its value is within the required range.

Let the magnetizing current in phase *a* be i_{am}, then the following relationship holds

$$\begin{aligned} i_{am} + \frac{2}{3} i_{ao} &= i_{a1} \\ i_{am} - \frac{1}{3} i_{ao} &= i_{a2} \end{aligned} \tag{18}$$

Either equation can be used to calculate the magnetizing current.

5.2 Magnetizing Current Minimization

The magnetizing current can be minimized by balancing the voltage applied across the tapped reactor. Among the seven switching states in Table I, states (0, 0), ($V_{dc}/2$, $V_{dc}/2$), and (V_{dc}, V_{dc}) have no effect on the magnetizing current, while the other four states can either increase or decrease the magnetizing current. Since states 2' and 4' are not used, there is no usable per-phase redundant state. Thus, the magnetizing current of each phase cannot be adjusted independently. In this paper, a technique similar to the joint-phase redundant states selection (JRSS) method proposed in [7] is used to minimize the magnetizing currents.

The concept behind JRSS is that for a three-phase inverter, the line-to-ground voltages of all phases may be changed simultaneously without affecting the load voltages since the terms that are common in all phases will cancel when looking at the line-to-neutral voltages or line-to-line voltages.

The current minimization procedure is as follows. At the beginning of each switching period, the magnetizing current for each phase is calculated. Suppose the commanded voltage levels are s_i, where $i = a, b, c$, and $0 \le s_i \le 6$. The number of available joint redundant states is

$$k = \min(s_i) + 6 - \max(s_i). \tag{19}$$

Each redundant state specifies the three-phase active filter voltage levels. Based on Table I, the voltage applied across the reactor for each phase, and whether the magnetizing current increases, decreases, or does not change can be determined. If the magnetizing inductance L_m is known, the change in the current (for phase a) can be calculated as

$$\Delta i_{am} = \frac{v_{a1} - v_{a2}}{L_m} \delta t \tag{20}$$

where v_{a1} and v_{a2} are voltages at the two terminals of the reactor, and δt is the duration of the state. The switching state that results in the minimum three-phase total magnetizing current is selected.

6. SIMULATION RESULTS

Numerical simulations have been conducted in the Advanced Continuous Simulation Language (ACSL) to validate the proposed topology. The example system has a rated line-to-line voltage of 306 V and a three-phase six-pulse diode rectifier with a 50 Ω dc load. The rated dc capacitor voltage of the active filter is 500 V. The three-phase tapped reactor has a leakage inductance of L_l = 50 μH, winding resistance r = 0.1 Ω, and mutual inductance L_M = 100 mH. The active filter interface inductance is 1 mH.

To further evaluate the performance of the proposed active filter, a real-time simulation model for a naval ship power system is also implemented, which has a rated voltage of 4.16kV. The modeling is based on the real time simulator RTDS® [13], which is a fully digital electromagnetic transients power system simulator that operates in real time. Because the solution is in real time, the simulator can be connected directly to a hardware controller or other devices. Thus, real-time simulation provides a convenient way for network-level power system analysis and equipment test.

The implementation of the proposed active power filter model in RTDS is quite different from simulation design with regular non-real-time continuous/discrete simulators. On the one hand, technical difficulties arise due to hardware limitations. The inherent computational delay (75 μs in the setup) may cause instability for the close-loop

controller, and the issue must be addressed with appropriate choice of control algorithms. The switch model, which is designed mainly for operation under fundamental frequency conditions, must be properly configured to work at high switching frequency and pass harmonic currents. On the other hand, the parallel structure of the current regulator makes it suitable to be implemented on the platform, because different harmonic channels can be processed in parallel by multiple processors.

Figures 5 and 6 show the *a*-phase operation of the active filter with the rectifier load. As can be seen, the load current i_{aL} contains a significant amount of harmonics. The active filter produces multilevel voltages that generate a current i_{af} to cancel the harmonic contents. The compensated source current i_{as} contains much less harmonics than i_{aL}. The total harmonic distortion of the load current is 25.1%, which is reduced to about 9.4% in the compensated source current. Since a first-order prediction is used for current regulation, the source current still contains a certain amount of higher-frequency components. However, they are generally not a concern and can easily be removed by passive filters.

The *a*-phase converter-side line-to-neutral output voltage v_{af} from the ACSL simulation is shown in Fig. 7. Multiple voltage levels give the voltage a smooth shape which reduces injection current ripple. Also shown in Fig. 7 is the reactor output terminal to dc ground voltage v_{ag}, which has seven distinct levels. Note that because of joint redundant state selection, common-mode components are added to the line-to-ground voltages, which cause the irregular shape of v_{ag}.

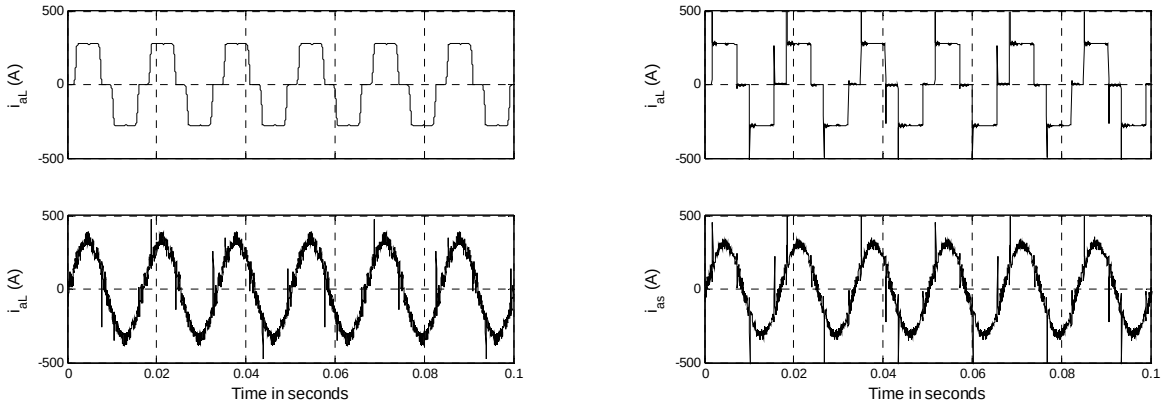

(a) (b)

Fig. 5. Load current and compensated current: (a) ACSL simulation; (b) RTDS.

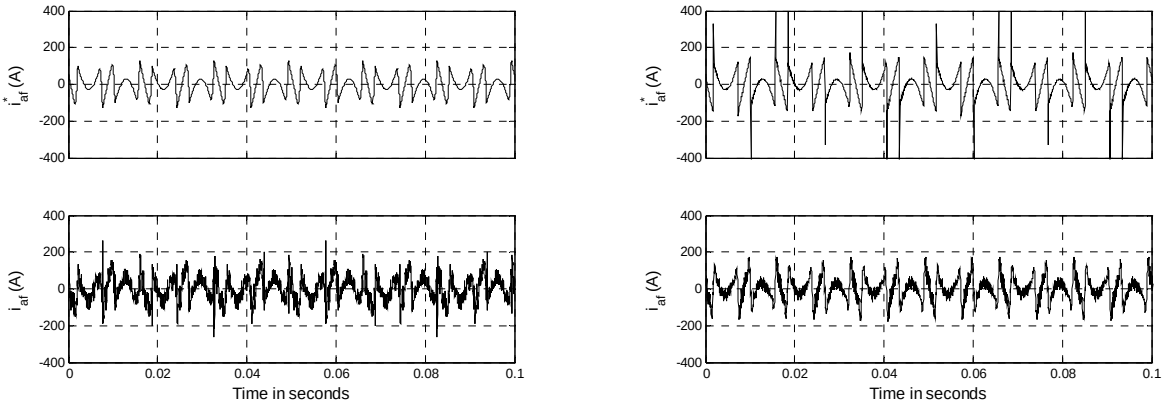

(a) (b)

Fig. 6. Reference and actual injection currents: (a) ACSL simulation; (b) RTDS.

The effectiveness of the magnetizing current control is tested in the ACSL simulation and illustrated in Fig. 8. The top part of Fig. 8 shows whether the JRSS current balancing algorithm is turned on or off, and the bottom part shows the magnetizing current in phase *a*. Initially the balancing is on and it can be seen that the magnetizing current is kept within a small range with a very low dc component. At time *t*

= t_{off}, the balancing algorithm is turned off, and the magnetizing current drifts away from zero and keeps decreasing. In practice, a large magnetizing current can cause the iron core to saturate and eventually damage the reactor and switching devices. When the balancing method is turned on again at $t = t_{on}$, the magnetizing current returns to its minimum value. Similar results are obtained for phase *b* and phase *c*.

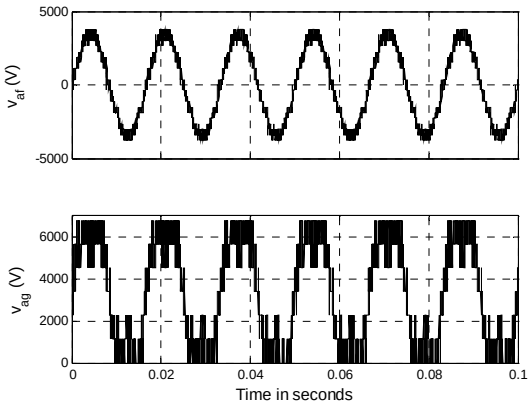

Fig. 7. Converter output voltages.

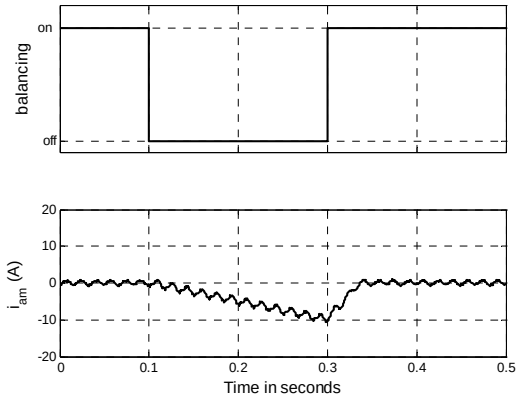

Fig. 8. Magnetizing current with and without balancing algorithm.

7. CONCLUSIONS

A topology based on tapped reactors for use in the parallel operation of active filters is presented in this paper. This reduces current stress of the switching devices by distributing the compensation current. This topology can also achieve seven output voltage levels and significantly reduce switching frequency harmonics. A detailed model of the tapped reactor is analyzed to show the relationship between reactor input and output voltages. To minimize reactor magnetizing currents, a joint redundant state selection method is used to balance the voltage across the reactor. Simulation results and real time implementation on a real time digital simulator platform confirm the effectiveness of the proposed topology and control strategies.

8. ACKNOWLEDGMENT

The financial support from the National Science Foundation, USA partly under the grant ECCS #0348221 is gratefully acknowledged by the authors for the study reported in this paper.

9. REFERENCES

1. B. Singh, K. Al-Haddad, and A. Chandra, “A Review of Active Filters for Power Quality Improvement,” *IEEE Transactions on Industrial Electronics*, volume 46, number 5, pages 960-971, October 1999.
2. M.E. Ortuzar, R.E. Carmi, et al., “Voltage-Source Active Power Filter Based on Multilevel Converter and Ultracapacitor DC Link,” *IEEE Transactions on Industrial Electronics*, volume 53, number 2, pages 477-485, April 2006.

3. Z. Du, L.M. Tolbert, and J.N. Chiasson, "Active Harmonic Elimination for Multilevel Converters," *IEEE Transactions on Power Electronics*, volume 21, number 2, pages 459-469, March 2006.
4. M.E. Ortuzar, R.E. Carmi, et al., "Voltage-source active power filter based on multilevel converter and ultracapacitor DC link," *IEEE Transactions on Industrial Electronics*, volume 53, number 2, pages 477-485, April 2006.
5. B.R. Lin and T.Y. Yang, "Analysis and implementation of a three-level active filter with a reduced number of power semiconductors," *IEE Proceedings on Electric Power Applications*, volume 152, number 5, pages 1055-1064, September 2005.
6. M. Glinka, "Prototype of multiphase modular-multilevel-converter with 2 MW power rating and 17-level-output-voltage," *IEEE PESC 04*, volume 4, pages 2572-2576, 2004.
7. J. Huang and K.A. Corzine, "Extended Operation of Flying Capacitor Multilevel Inverters," *IEEE Transactions on Power Electronics*, volume 21, pages 140-147, January 2006.
8. F. Ueda, K. Matsui, et al., "Parallel-connections of pulsewidth modulated inverters using current sharing reactors," *IEEE Transactions on Power Electronics*, volume 10, number 6, pages 673-679, November 1995.
9. H. Mori, K. Matsui, et al., "Parallel-connected five-level PWM inverters," *IEEE Transactions on Power Electronics*, volume 18, number 1, part 1, pages 173-79, January 2003.

10. K. Matsui, Y. Kawata and F. Ueda, "Application of parallel connected NPC-PWM inverters with multilevel modulation for AC motor drive," *IEEE Transactions on Power Electronics*, volume 15, number 5, pages 901-907, September 2000.
11. S. Ogasawara. J. Takagaki, et al., "Novel Control Scheme of a Parallel Current-Controlled PWM Inverter," *IEEE Transactions on Industry Applications*, volume 28, number 5, pages 1023-1030, September 1992.
12. S. Bhattacharya, T.M. Frank, et al., "Active Filter System Implementation," *IEEE Industry Applications Magazine*, volume 4, number 5, pages 47-63, September 1998.
13. P. Forsyth, T. Maguire, R. Kuffel, "Real time digital simulation for control and protection system testing," *Proceedings of the IEEE Power Electronics Specialists Conference*, volume 1, pages 329-335, 2004.

Paper II

Multiple Reference Frame-based Control of Three-Phase PWM Boost Rectifiers under Unbalanced and Distorted Input Conditions

Peng Xiao, Keith A. Corzine, and Ganesh K. Venayagamoorthy
Real-Time Power and Intelligent Systems Laboratory
Department of Electrical and Computer Engineering
University of Missouri-Rolla, Rolla, MO, 65401 USA
pxfx7@umr.edu, keith@corzine.net and gkumar@ieee.org

ABSTRACT

Many control algorithms and circuits for three-phase pulse width modulation active rectifiers have been proposed in the past decades. In most of the research works, it is often assumed that the input voltages are balanced or contains only fundamental frequency components. In this paper, a selective harmonic compensation method is proposed based on an improved multiple reference frame algorithm, which decouples signals of different frequencies before reference frame transformation. This technique eliminates interactions between the fundamental-frequency positive-sequence components and harmonic and/or negative-sequence components in the input currents, so that the fast and accurate regulation of harmonic and unbalanced currents can be achieved. A decoupled phase-locked loop algorithm is used for proper synchronization with the utility voltage, which also benefits from the multiple reference frame technique. The proposed control method leads to considerable reduction in low-order harmonic contents in the rectifier input currents and achieves almost zero steady-state error through

feedback loops. Extensive experimental tests based on a fixed-point digital signal processor controlled 2 kW prototype are used to verify the effectiveness of the proposed ideas.

Keywords

active rectifier, harmonic compensation, multiple reference frame, phase-locked loop

1. INTRODUCTION

Three-phase voltage-source pulse width modulation (PWM) rectifiers have gained enormous popularity in the past two decades. In many motor drive and power supply applications, they have been replacing traditional diode/thyristor bridge rectifiers as the front end ac/dc interface due to their low line current distortion and high power factor. Although there are constant efforts to improve the power quality of diode/thyristor rectifiers, either through additional circuits [1-3] or using active filters [4], PWM rectifiers are still one of the most viable solutions for many applications, especially when bidirectional power flow is required [5].

The main benefits of PWM converters come from the fact that their switching devices operate at a frequency many times higher than the system fundamental frequency. This enables the converter to have fast response and close regulation of the dc voltage. Since the switching noise can be easily eliminated by passive filters, the supply currents drawn from the utility network are nearly sinusoidal in normal conditions. In addition, the PWM rectifier can maintain good power factor through a wide load range.

The claim that PWM rectifiers draw little low-order harmonic current, however, is seldom true when the input voltages are unbalanced or contain harmonics. The three-

phase power source, be it the power grid or a stand-alone generator, is rarely ideal in practical situations. If the rectifier control scheme is not designed properly to account for these non-ideal situations, the three-phase input currents can indeed contain low-order harmonics. It has been pointed out that with unbalanced input voltages the rectifier dc output voltage may contain second-order harmonic ripple, which in turn causes third-order non-zero-sequence harmonics in the input currents [6]. Although the magnitude of these harmonics is much lower compared to those generated by the diode/SCR counterparts, they can lead to lower power quality and may require additional passive filters to meet harmonic regulatory standards such as IEEE-519. Furthermore, non-ideal input voltage conditions may interfere with the converter controller and degrade its performance in achieving the two major objectives: dc voltage regulation and power factor correction. Laboratory experiments have shown that large amount of harmonics in the line voltages can cause sub-harmonic resonance and affect the stability of the rectifier control.

The performance of PWM rectifiers under distorted input conditions varies greatly depending on the control scheme adopted. Harmonics and unbalance in the input voltages create a disturbance to the control, and very few control algorithms can provide a wide enough bandwidth to effectively suppress them. This is especially true for controls with slower current regulators.

Several methods have been proposed to improve the operation of PWM rectifiers under unbalanced input voltage conditions. Early research focused on the analysis of rectifier behavior under these conditions, and attempted to alleviate the situation by proper design of input inductors and dc capacitors [6]. In [7], a feed-forward control

circuit was proposed, which used analog/digital components to generate appropriate PWM gating signals based on an unbalanced transfer matrix. Although the control had a simple implementation, its lack of feedback made the compensation sensitive to sensor errors and component variations. Based on symmetrical component theory, a feed-forward control strategy was proposed in [8] to eliminate harmonics caused by unbalanced input conditions. One of its main drawbacks is that unity power factor cannot be achieved. A dual current controller was proposed in [9], which utilized two synchronous reference frames (SRFs) to separately regulate the positive and negative sequence currents. The use of two SRFs achieved very good control performance of the negative sequence components. However, the separation of the positive and negative SRFs was implemented with either low-pass filters or notch filters, whose limitations are detailed in Section 3.

Some recently developed rectifier control algorithms also consider harmonics in the source voltages. A generalized model was derived in [10] to address the control issues caused by unbalanced and/or harmonic input conditions. Effects of harmonics on rectifier control was investigated in detail, but the compensation scheme only considered unbalanced inputs. Elimination of low-frequency harmonics in active rectifiers was also considered in [11], which attributed the sources of harmonics to pulse-width limits, improper PWM patterns and dead time. A predictive cancellation algorithm was proposed in [12] to reduce harmonics in the rectifier input currents. However, due to the algorithm's open-loop nature, its performance was sensitive to sensor errors and control time delay.

With advances in the design of active filter controls, a new trend in harmonic current regulation is the use of selective harmonic compensation techniques, which target only a selected group of harmonic components, instead of trying to regulate signals in a wide spectrum. These techniques can be roughly classified into two categories based on the frame of reference they employ, although it has been proven that some of the methods are just equivalent implementations in different reference frames [13-14].

Several stationary reference frame based control methods have been proposed and found applications in active filters, voltage source rectifiers, uninterruptable power supplies (UPS), and static var compensators (STATCOMs) [13-19]. The majority of these techniques are based on a form of resonant notch filter transfer function. In some cases, an integrator or proportional-integrator (PI) stage is also incorporated in the transfer function. Another stationary frame based method was the adaptive selective harmonic elimination (ASHE) algorithm [20], which could eliminate certain harmonic components by slowly adjusting weight parameters using a least mean square algorithm.

The other category of selective harmonic control methods are based on rotating reference frames. In [21], Schauder et al. proposed a multiple reference frame based controller for active filters and power line conditioners. A similar implementation was set forth in [22] for active filter control.

In this paper, a novel control algorithm is proposed to eliminate the low-order harmonic components in the ac currents of grid-tied converters when input ac voltages are unbalanced or contain low-order harmonics. Based on multiple reference frame theory, the proposed method improves existing implementation to achieve faster dynamics and lower computational requirement. The main goal of the control is to

produce high-quality balanced sinusoidal three-phase currents on the ac side in the presence of distorted input voltage conditions, thus avoid drawing harmonic or unbalanced currents from the utility system. The proposed harmonic elimination control method can be applied to both PWM rectifiers and grid-tied PWM inverters. In this paper, a 2 kW three-wire PWM boost rectifier system is used as an example to demonstrate its effectiveness.

The effects of distorted input conditions on rectifier control are briefly studied in Section 2, in which the control objectives of the proposed technique are also defined. In Section 3, the decoupled multiple reference frame algorithm is derived, and comparisons are made between existing techniques and the proposed method. Based on the MRF technique, a line synchronous algorithm is set forth in Section 4, where simulation results are used to demonstrate its effectiveness. Although the MRF-based harmonic compensation technique can be integrated with many basic rectifier control algorithms, a *P*-*Q* decoupled control scheme is adopted in this work and illustrated in Section 5. Implementation of the proposed algorithms in a digital signal processor (DSP) system is described in Section 6, where extensive test results are presented.

2. BEHAVIOR OF RECTIFIER CONTROL UNDER UNBALANCED AND DISTORTED CONDITIONS

2.1 Circuit Description

The typical circuit diagram of a three-phase PWM voltage source boost-type rectifier is shown in Fig. 1. Therein, the three legs of a three-phase IGBT bridge are connected to the power grid through an inductor L (with series resistance r). In most control schemes, the output dc voltage v_{dc} and the input source voltages $\mathbf{v}_s = [v_{as}, v_{bs}, v_{cs}]^T$

and currents $\mathbf{i}_s = [i_{as}, i_{bs}, i_{cs}]^T$ are sensed and then used to determine the proper PWM gating signals S_a, S_b, S_c and their complements. In a three-wire system as shown in Fig. 1, since there is no zero-sequence current path, the three-phase quantities are not independent. Therefore, only two line-to-line voltages (v_{ab} and v_{bc}) and two currents (i_{as} and i_{bs}) need to be sensed. Switching at a high frequency, the IGBT legs produce voltages at the rectifier terminals, whose average values $\mathbf{v}_r = [v_{ar}, v_{br}, v_{cr}]^T$ would form a set of three-phase balanced sinusoidal voltages under ideal conditions.

It should be noted that since there is no neutral wire, the zero-sequence ac current is always zero, no matter what source voltages are applied. Therefore, it is convenient in the following derivation to omit the zero-sequence component, and only q- and d-axis quantities are considered in each reference frame.

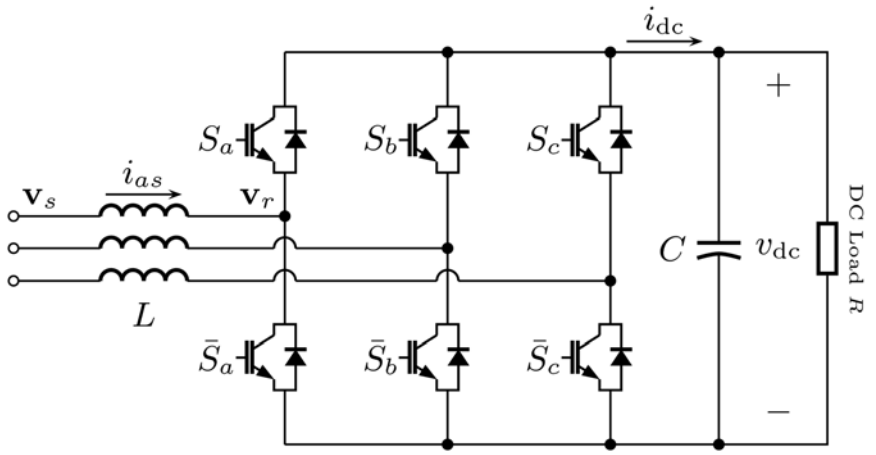

Fig. 1. Circuit diagram of a three-phase boost-type rectifier system.

2.2 Synchronous Reference Frame Equivalent Circuit

A brief analysis of the behavior of the rectifier is helpful for the understanding of the effects of unbalanced and distorted input conditions. The state-space model of the

above circuit can be established in the synchronous reference frame, in which the *abc* variables are transformed into *qd* variables in a rotating coordinate.

A two step transformation process is often seen in the literature, in which *abc* variables were first translated into stationary *qd* variables with a constant matrix, then translated into the synchronous reference frame with a time-varying matrix. In this paper, a direct approach is taken as follows

$$\begin{bmatrix} f_q \\ f_d \end{bmatrix} = \frac{2}{3}\begin{bmatrix} \cos(\theta) & \cos(\theta - 2\pi/3) & \cos(\theta + 2\pi/3) \\ \sin(\theta) & \sin(\theta - 2\pi/3) & \sin(\theta + 2\pi/3) \end{bmatrix}\begin{bmatrix} f_a \\ f_b \\ f_c \end{bmatrix} \tag{1}$$

where f denotes any three-phase quantities such as voltages, currents, or flux linkages, and θ is the phase angle of the a-phase utility voltage $\mathbf{v}_s$. As mentioned earlier, it is assumed that zero-sequence component is negligible, therefore

$$f_c = -f_a - f_b \tag{2}$$

The reverse transformation is

$$\begin{bmatrix} f_a \\ f_b \\ f_c \end{bmatrix} = \begin{bmatrix} \cos(\theta) & \sin(\theta) \\ \cos(\theta - 2\pi/3) & \sin(\theta - 2\pi/3) \\ \cos(\theta + 2\pi/3) & \sin(\theta + 2\pi/3) \end{bmatrix}\begin{bmatrix} f_q \\ f_d \end{bmatrix} \tag{3}$$

The state-space equations for the ac side circuit are

$$\begin{aligned} Lpi_{qs} &= v_{qs} - i_{qs}r - \omega_e L i_{ds} - v_{qr} \\ Lpi_{ds} &= v_{ds} - i_{ds}r + \omega_e L i_{qs} - v_{dr} \end{aligned} \tag{4}$$

where p denotes differentiation with respect to time, $\omega_e = p\theta$ is the electrical angular speed of the utility voltage, and [v_{qs}, v_{ds}], [i_{qs}, i_{ds}] and [v_{qr}, v_{dr}] are the results obtained when $\mathbf{v}_s$, $\mathbf{i}_s$, and $\mathbf{v}_r$ are transformed into the synchronous reference frame, respectively.

For the dc side circuit, the following equation holds,

$$Cpv_{dc} = i_{dc} - \frac{v_{dc}}{R} \tag{5}$$

In (5), C is the capacitance of the dc linkage capacitor, and R is the equivalent resistance of the dc load. The two sides are related through instantaneous power balance

$$i_{dc} = \frac{3}{2}\frac{\left(v_{qr}i_{qs} + v_{dr}i_{ds}\right)}{v_{dc}} \tag{6}$$

Fig. 2 shows the ac side circuit diagram in SRF. It can be shown that if the input voltage $\mathbf{v}_s$ are balanced and free of harmonics, v_{qs} and v_{ds} become dc quantities. A controller can be designed to determine v_{qr} and v_{dr}, which are also dc quantities in steady states.

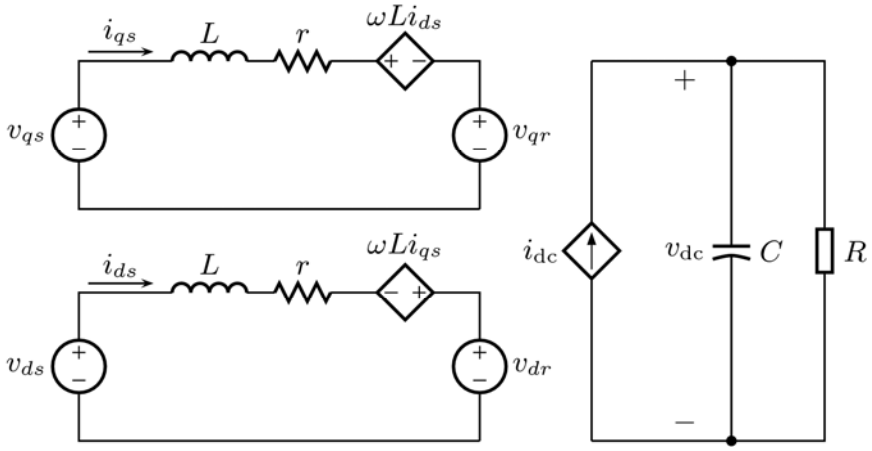

Fig. 2. Equivalent circuit diagram of the rectifier system in the synchronous reference frame.

However, if the input voltages $\mathbf{v}_s$ are unbalanced or contain harmonic components, v_{qs} and v_{ds} are no longer constant and contain a series of sinusoidal components, which act as disturbances to the system. In this case, the operating point of the system is no longer fixed, and the controller must have a very large bandwidth to

suppress these disturbances, otherwise harmonic components will appear in the state variables, i.e., the input ac currents and output dc voltage. It should be noted that the input inductor of the rectifier circuit often has a relatively low inductance. Therefore, even a small amount of harmonics in $\mathbf{v}_s$ can create large harmonic currents if $\mathbf{v}_r$ does not have the same canceling components. To address the issue of non-ideal input conditions, several approaches have been proposed [23]. The constant power method tries to maintain a constant input power (assuming the dc load is also constant), thus eliminating ripple in the output dc voltage. The constant resistance method regulates the rectifier so that it appears as a three-phase balanced resistive load. In this work, the control objective is to maintain balanced sinusoidal three-phase input currents, even when the input voltages are unbalanced and/or contain harmonics.

3. MULTIPLE REFERENCE FRAME HARMONIC CONTROL SCHEME

3.1 Overview of the Multiple Reference Frame Theory

The concept of multiple reference frames was set forth several decades ago and was initially used in the analysis of electric machinery. In [24], Krause established the basic architecture of MRF and considered its application in the analysis of symmetrical induction machines. It was shown that the MRF method allowed simplified steady-state analysis of machine operations under unbalanced or non-sinusoidal voltage conditions. Later, Sudhoff et al. presented MRF-based analysis of a variety of other electric machines, including unsymmetrical induction machines [25], multistack variable-reluctance stepper motors [26], and brushless dc motors [27]. These machines are difficult to model with conventional methods due to asymmetry or non-sinusoidal back emf. MRF provided a means to keep state variables of the model constant in steady state

so that the model equations could be readily linearized. Recently, MRF was also employed in the identification of inter-turn faults in induction machine stators [28].

It is interesting to note that although MRF has found many applications as an analysis tool, its use in real-time controllers has not received much attention. This is primarily due to the fact that, i) significant computation arises from the need for reference frames transformations; ii) the dynamic performance of most existing MRF based controllers is not satisfactory; and iii) accurate synchronization with utility voltage is required.

With the advances in modern DSP design, commercial off-the-shelf DSP chips today have significantly improved their computational power through increased clock speed and parallel operation. Thus, the computational requirement is no longer a determining factor. Herein, the issues of performance and synchronization will be addressed.

3.2 Multiple Reference Frames for Arbitrary Three-Phase Signals

The synchronous reference frame is commonly used in the control of PWM rectifiers and inverters. By transforming the time-varying three-phase sinusoidal voltage and current signals to this rotating reference frame using (1), these signals become dc quantities in steady state. It is thus much easier to design the controller to achieve zero steady-state error. The same concept can be naturally extended to cases where the signals are unbalanced and/or contain harmonics. Let $\mathbf{v} = [v_a, v_b, v_c]^T$ be a set of three-phase periodic voltage signals with arbitrary waveforms. As long as all three signals are periodic with the same base frequency ω_e, each can be expressed as the sum of a series of harmonics using the Fourier transform

$$v_j = \sum_{k=0}^{\infty} A_{jk} \cos\left(k\omega_e t + \phi_{jk}\right) \tag{7}$$

where $j = a$, b, and c; A_{jk} and ϕ_{jk} are respectively the magnitude and phase angle of the k-th harmonic component in phase j.

For each harmonic frequency $f_k = k\omega_e/2\pi$, symmetrical component theory can be applied. No matter what magnitude or phase angles each phase component has at this frequency, there exist three sets of symmetrical components that can uniquely represent the three-phase signals at f_k,

$$\begin{bmatrix} A_{ak}\cos\left(k\omega_e t + \phi_{ak}\right) \\ A_{bk}\cos\left(k\omega_e t + \phi_{bk}\right) \\ A_{ck}\cos\left(k\omega_e t + \phi_{ck}\right) \end{bmatrix} = A_k^+ \begin{bmatrix} \cos\left(k\omega_e t + \phi_k^+\right) \\ \cos\left(k\omega_e t + \phi_k^+ - 2\pi/3\right) \\ \cos\left(k\omega_e t + \phi_k^+ + 2\pi/3\right) \end{bmatrix} + A_k^- \begin{bmatrix} \cos\left(k\omega_e t + \phi_k^-\right) \\ \cos\left(k\omega_e t + \phi_k^- + 2\pi/3\right) \\ \cos\left(k\omega_e t + \phi_k^- - 2\pi/3\right) \end{bmatrix} + A_k^0 \begin{bmatrix} \cos\left(k\omega_e t + \phi_k^0\right) \\ \cos\left(k\omega_e t + \phi_k^0\right) \\ \cos\left(k\omega_e t + \phi_k^0\right) \end{bmatrix} \tag{8}$$

If the zero-sequence component is assumed to be zero, the harmonic contents at frequency f_k can be represented by two balanced sets of quantities with the same electrical angular velocity $k\omega_e$: one set ($A_k^+ \angle \phi_k^+$) has positive sequence and its vector rotates counterclockwise in the vector plane, while the other set ($A_k^- \angle \phi_k^-$) has negative sequence and its vector rotates in the clockwise direction.

From the above analysis, it is clear that a set of periodic three-phase quantities can be viewed as a sum of multiple rotating vectors in the vector plane. Generally speaking, for each harmonic frequency f_k ($k = 1, 2 \ldots, \infty$), two vectors may exist that rotate at the same electrical angular velocity $k\omega_e$ but in opposite directions.

A reference frame can be intuitively viewed as a rotating coordinate in the vector plane, which has a *q*-axis and a perpendicular *d*-axis. The *q*- and *d*-axis quantities of a vector viewed in that reference frame are simply the projection of the vector onto the two axes. Reference frame transformation, in this sense, is a change of the viewer's perspective from the stationary coordinate to a rotating one.

As proven in [24], if a balanced set appears in any reference frame, there is another reference frame wherein this balanced set will appear as constants. Therefore, when **v** is transformed into a reference frame that is rotating counterclockwise at velocity $k\omega_e$, the positive-sequence vector of the *k*-th harmonic in **v** will appear as standing still because it is moving in the same velocity and direction as the reference frame. In other words, transformation of this vector gives constant *q*- and *d*-axis quantities. A positive sequence vector that is rotating at velocity $m\omega_e$ ($m \geq 0$, $m \neq k$) will appear as sinusoidal terms with a frequency of $2\pi(m-k)\omega_e$. A negative sequence vector that is rotating with $m\omega_e$ will appear as sinusoidal terms with a frequency of $2\pi(m+k)\omega_e$.

In summary, when the zero-sequence component is not considered, a periodic three-phase signal can be decomposed into a sum of balanced three-phase sets; each can be of different harmonic frequencies, and can have either positive sequence or negative sequence. For each harmonic set, there exist one and only one reference frame into which the component can be transformed to be dc quantities. Conversely, when the signal is transformed into a specific reference frame, only one harmonic set becomes dc quantities, and all other sets become sinusoidal terms whose frequency is determined by the relative angular velocity between the set and the reference frame.

3.3 Existing MRF-based Control Methods

One technique based on multiple reference frames for active filter control was proposed in [22], where a current regulator was constructed and each harmonic component was regulated on its own rotating reference frame. A similar technique was proposed in [21] which integrated a PI controller in the MRF structure for each frequency of interest. Although these methods are simple and straightforward to implement, they suffer from a serious drawback, i.e., interference between different reference frames.

As described earlier, a balanced harmonic set $A_m \angle \phi_m$ that is not in synchronization with the reference frame becomes sinusoidal terms after the transformation. The frequency of the terms is determined by the relative velocity of the set and reference frame, and their magnitude are unchanged by the transformation. In [21], the original three-phase signals were sent to each reference frame so that the transformation result contained not only the desired dc component, but also a variety of sinusoidal terms. This inevitably affects the accuracy and dynamic performance of the controller since even in steady state the state variables of the system were not constant. In each reference frame, the system was constantly perturbed by a group of sinusoidal disturbances.

One way to alleviate this situation is to attenuate at least the dominant component with filters, as was done in [22]. Therein, a low-pass filter was constructed to reduce the magnitude of the positive sequence fundamental components, which was the dominant one in the nonlinear load currents. The output signal of the filter was then processed by MRF. Although filters can indeed partially reduce interactions among reference frames, their use comes with a price, i.e. the degraded dynamic response of the system. This is

especially true when simple low-order filters are used. In fact, as will be shown in the next section, a difficult compromise has to be made between the attenuation and dynamic performance.

3.4 MRFSER

A novel multiple reference frame synchronous estimator/regulator (MRFSER) was set forth by Chapman and Sudhoff in [29]. The technique was applied to the optimal control of permanent magnet synchronous machine drives. Fig. 3 depicts the block diagram of the MRF synchronous estimator, which is essentially the same diagram as shown in Fig. 3 of [29], except that in the original figure an integrator with unity negative feedback was used, instead of a low-pass filter. It can be shown that the integrator with unity negative feedback loop has a transfer function

$$H(s) = \frac{1}{s / G_e + 1} \tag{9}$$

which is identical to that of a first-order low-pass filter with unity dc gain and a cutoff frequency of G_e. Thus, Fig. 3 can be seen as a generalized version of the MRF synchronous estimator in [29].

As can be seen in Fig. 3, a three-phase current signal is processed by several parallel channels, each representing a frame of reference (α, β, … Ω). Unlike conventional MRF techniques which multiply the raw signal directly with transformation matrices ($\mathbf{K}_\alpha, \mathbf{K}_\beta, \ldots, \mathbf{K}_\Omega$), MRFSER subtracts the sum of all estimated components from the original signal, and adds to it the estimated component resulted from the specific reference frame the signal is being transformed into. In the steady state, this feedback network allows only one component to pass through each reference frame, and that

component is exactly the one that is in synchronization with the reference frame. Therefore, the scheme essentially decouples all the different reference frames so that the output of each channel contains only constant quantities, which are the *q*- and *d*-axis values of a balanced harmonic set that rotates synchronously with the reference frame. In other words, the MRFSER is capable of extracting cleanly each harmonic component in the input signal. This is a feature that can not be achieved by using either low-pass filters or notch filters. It is important to note that although harmonic contents considered in [29] were assumed to be balanced, the general idea can be extended to three-phase periodic signals with arbitrary waveforms.

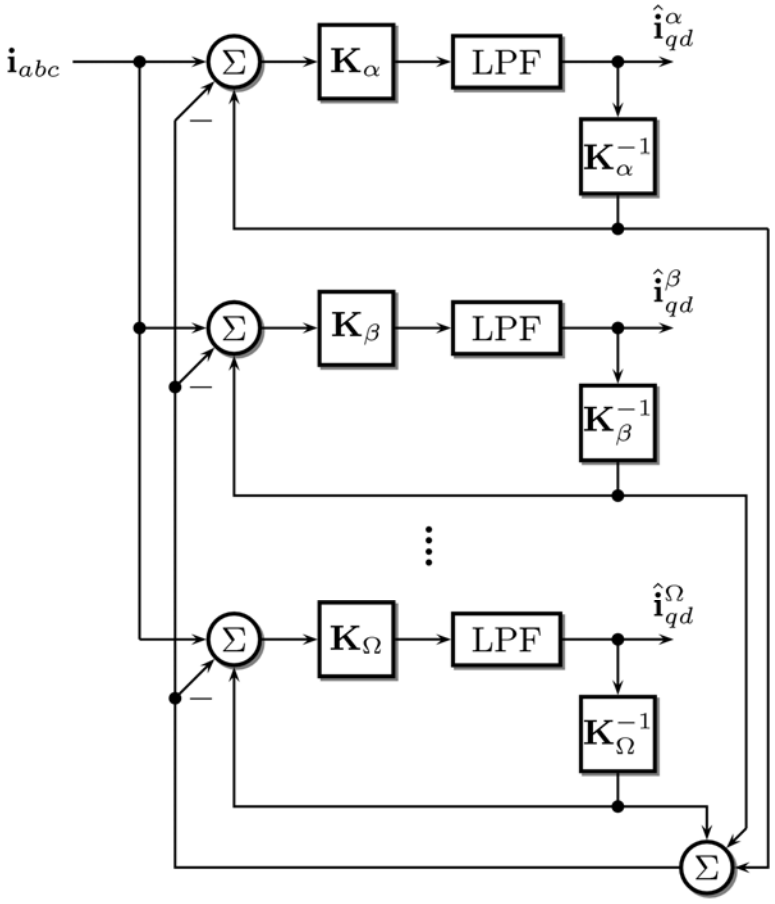

Fig. 3. Block diagram of the multiple reference frame estimator/regulator.

Formal mathematical justification was presented in [29], which shows that the error of the estimator will converge exponentially to zero if the input is constant and all harmonic components are considered in the MRFSER structure. The rate of the convergence depends on the number of channels (n) and the low-pass filter. In the case of simple first-order low-pass filters, the decay rate is $n\omega_c$, where ω_c is the cutoff frequency of the filter.

Although MRFSER provided a fast and accurate means to estimate individual harmonic components in a three-phase periodic signal, it has not been widely adopted in practical applications. One drawback of the MRFSER implementation is that it requires very intensive computational power to perform the transformations of different reference frames. For each harmonic component, signals not only need to be transformed into the *qd* reference frame, they also need to be re-constructed by inverse transformation back into the *abc* forms. This would significantly increase the required computational efforts. Therefore, for practical implementation with DSPs, the MRFSER presents hardware and software challenges, especially when the number of harmonic channels is high.

3.5 Improved MRF Scheme

To apply MRFSER in rectifier control, one major challenge is to reduce the amount of calculations it requires. For three-phase utility-connected power converters, the following observations are made:

- The most dominant component in the converter currents is the positive sequence fundamental frequency component, which can have a magnitude tens of times higher than that of harmonic components.

- Unbalance can be a common phenomenon in the utility systems, and high magnitude of negative sequence fundamental component may exist.
- In most systems, even and triplen harmonics are not an issue. The dominant low-order harmonics are the 5^{th}, 7^{th}, 11^{th}, 13^{th}, etc. Furthermore, the higher the frequency is, the lower the magnitude is.
- If the signals are balanced, the 5^{th}, 11^{th}, ... harmonics have a negative sequence, while the 7^{th}, 13^{th}, ... harmonics have a positive sequence.
- If the signals are unbalanced, positive sequence 5^{th}, 11^{th}, etc. harmonics and negative sequence 7^{th}, 13^{th}, etc harmonics may exist, but they have very low amplitudes.

Based on these observations, a modified MRF scheme is proposed in this paper. The block diagram of the scheme is shown in Fig. 4, where the superscript 1*p* is used to denote fundamental frequency positive sequence component, 1*n* stands for fundamental frequency negative sequence component, 5*n* stands for 5^{th} harmonic negative sequence component, and so on.

Before the input current signal is transformed into reference frame 1*p*, the output of reference frame 1*n* is reconstructed and subtracted from the input signal. Similarly, the output of reference frame 1*p* is reconstructed and subtracted from the input signal that goes into reference frame 1*n*. The estimated 1*p* components are

$$\hat{\mathbf{i}}_{qd}^{1p} = LPF\left[\mathbf{K}_{1p}\left(\mathbf{i}_{abc} - \mathbf{K}_{1n}^{-1}\hat{\mathbf{i}}_{qd}^{1n}\right)\right] \tag{10}$$

and the estimated 1*n* components are

$$\hat{\mathbf{i}}_{qd}^{1n} = LPF\left[\mathbf{K}_{1n}\left(\mathbf{i}_{abc} - \mathbf{K}_{1p}^{-1}\hat{\mathbf{i}}_{qd}^{1p}\right)\right] \tag{11}$$

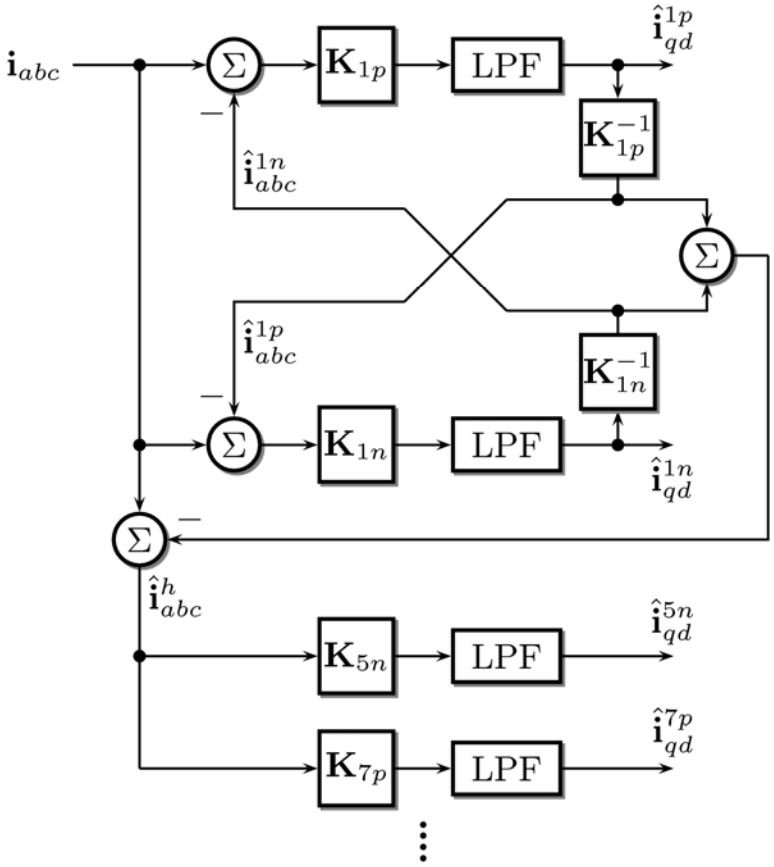

Fig. 4. Block diagram of the proposed multiple reference frame scheme.

Compared with MRFSER, it can be seen that only fundamental frequency components are involved in the feedback network, and no reconstruction of harmonic estimations is needed.

In this way, the input current is divided into three major components, i) the positive sequence fundamental frequency component $\mathbf{i}^{1p}$, ii) the negative sequence fundamental component $\mathbf{i}^{1n}$ caused by imbalance, and iii) the remaining components $\mathbf{i}^{h}$ which are harmonics. All reference frames that process harmonics share the same input signal, which is

$$\mathbf{i}^{h} = \mathbf{i} - \mathbf{i}^{1p} - \mathbf{i}^{1n} \tag{12}$$

If the input signal does not contain any harmonic components, this structure will cleanly extract the positive and negative sequence fundamental frequency components. Since harmonics are not considered in the feedback network, in reality there are some interferences between different reference frames. However, the low magnitude of the harmonics means that their effects are small, as is shown below.

3.6 Simulation Results

To demonstrate the effectiveness of the proposed MRF scheme, a computer simulation was performed and comparisons were made between three MRF implementations, the conventional filter based method, MRFSER, and the proposed scheme.

In the simulation test, a 60 Hz three-phase voltage signal was processed with the three MRF schemes. In the signal, phase *a* had a magnitude of 197V, which was 10% higher than that of phase *b* and *c*. In addition, the signal contained 5% negative sequence 5^{th} harmonic component. To test the dynamic behavior of the methods, a step change occurred at time $t = 0.05$ s when the magnitude of the signal dropped by 30%.

The simulation results are reported in Fig. 5. Therein, the left column depicts the *q*-axis quantity of the extracted positive sequence fundamental components ($1p$), the right column depicts the extracted *q*-axis values of the negative sequence fundamental components ($1n$) and 5^{th}-order harmonic component ($5n$).

The two plots shown in the first row of Fig. 5 illustrate the results of the conventional MRF method. To reduce the interactions between different reference frames, a low-pass filter with cutoff frequency $\omega_c = 10$ Hz was used. It can be seen in Fig 5 (b) that the extracted $1n$ and $5n$ components still contain very large amount of ripple

caused by the dominant 1p component. Although decreasing the cutoff frequency can reduce the amplitude of the ripple, it also further deteriorates the dynamic performance of the system, which is already very poor as shown in Fig. 5 (a).

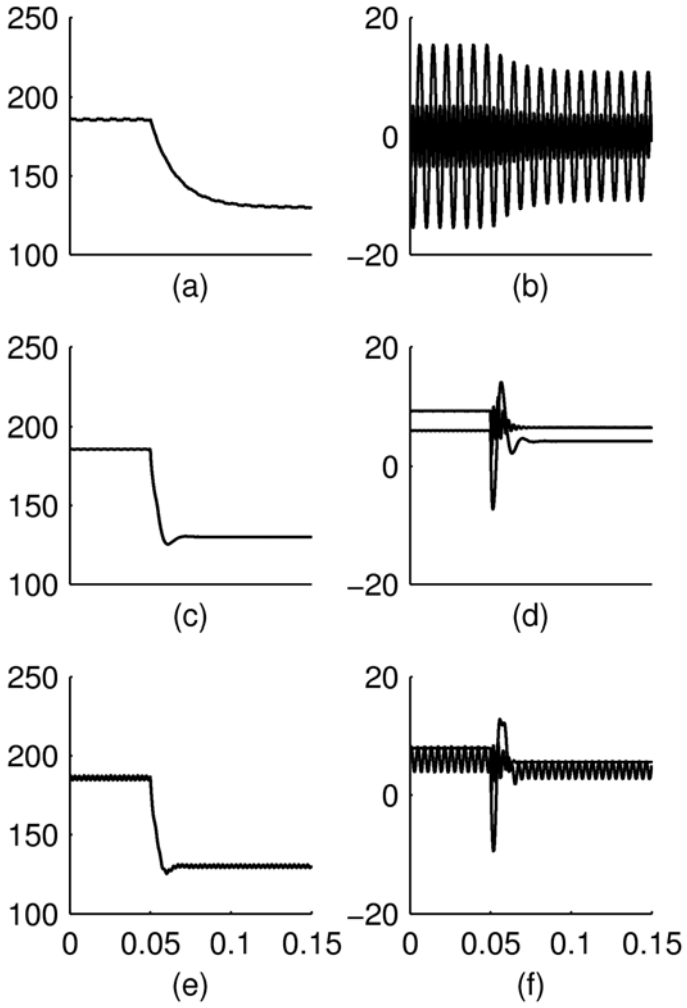

Fig. 5. Comparison of simulation results from three MRF-based methods. First row: conventional MRF; Second row: MRFSER; Last Row: proposed MRF scheme. Left column: estimated q-axis values of 1p component; Right column: estimated q-axis values of 1n and 5n components.

The results from the MRFSER method can be observed in the two plots shown in the second row of Fig. 5. In this study, a cutoff frequency of 60 Hz was selected for the

low-pass filters. It is clear that MRFSER achieved much better dynamic performance and could completely eliminate interferences between different reference frames. In steady state, the estimated *q*-axis quantities are all constant values in each reference frame.

Finally, the traces in the bottom row of Fig. 5 depict the behavior of the proposed MRF algorithm, which used the same cutoff frequency as in the MRFSER study. The dynamic responses compare nearly identically to those of MRFSER. In steady state, there was only a small amount of high frequency ripple in the 1*p* and 1*n* component, which is expected due to the fact that 5*n* is not included in the feedback network. Because the 5*n* component has a much lower magnitude compared with fundamental frequency components, its effects on them were negligible in most cases. On the other hand, since the input signal to 5*n* reference frame has no 1*p* or 1*n* components, the transformation results are nearly dc quantities.

It is interesting to note that the 5*n* component becomes a 360 Hz sinusoid in the 1*p* reference frame, while it appears as a 240 Hz sinusoid in the 1*n* reference frame. Since the same cutoff frequency was used for all low-pass filters, the magnitude of the ripple in the 1n reference frame is higher than that in the 1*p* reference frame.

Based on the study, it can be concluded that although the proposed MRF may introduce some ripple caused by harmonics, their impacts are very limited in practical situations. The dominant components, which are often the ones with fundamental frequency, are decoupled and removed. The proposed method simplifies the MRFSER structure and reduces computational requirement, without degrading dynamic performance.

It is important to mention that in some cases a harmonic component may have a significant enough magnitude to cause large ripple in other reference frames, and the proposed MRF method can be readily modified to include that harmonic channel in the feedback network.

4. MRF-BASE LINE SYNCHRONIZATION ALGORITHM

The tracking of phase and frequency information of the utility systems is an important aspect of most converter control algorithms that use SRF technique. Although small variations of the estimated system frequency normally may not cause problems for the control of fundamental frequency signals, they can introduce a lot more ripple in the *qd* quantities of higher-order harmonics.

For example, an estimation error of 0.5 Hz for the fundamental component would cause an error of 6.5 Hz for the 13th harmonic reference frame, and it is very difficult to remove such ripple with simple low-pass filters while keeping good dynamic performance. Thus, to achieve good performance using MRF, the frequency of the utility system must be accurately tracked.

A commonly-used line-synchronization technique for three-phase applications is the synchronous reference frame phase locked loop (SRF-PLL) method [30], in which the source voltages are transformed into the *qd* rotating reference frame, and a feedback loop is used to regulate the angular position of the reference frame so that either the *q*- or *d*-axis component becomes zero. The SRF-PLL gives satisfactory performance under ideal input conditions, i.e. when the source voltage is balanced and free of harmonics. However, imbalance and distortions in the source voltage can cause large oscillations in the extracted frequency and phase information. Even though these oscillation can be

attenuated by low-pass filters, this approach has a serious negative impact on the dynamic performance of the PLL. Therefore, this method is not appropriate for the proposed MRF-based harmonic compensation algorithm.

Recently, based on the conventional SRF-PLL, a novel improvement called the decoupled double synchronous reference frame PLL (DDSRF-PLL) was proposed [31], which utilized two synchronous reference frames to process the input voltages. The two reference frames have the same angular speed, but are rotating in opposite directions. Signals in the two reference frames are decoupled through a feedback network so that the interference between them can be totally eliminated. This key feature of the technique makes it possible to extract separately the fundamental-frequency positive-sequence component, which can then be used in the PLL stage. Through simulation and experimental results, the authors showed that the technique had excellent performance even when input voltages were highly unbalanced. The effect of harmonics on the PLL was also investigated and the results showed that they have very little negative impact.

In this paper, the same idea of DDSRF-PLL is adopted, but a different approach is taken for the implementation. Fig. 6 shows the control diagram of the proposed MRF-PLL scheme. It can be seen that the a decoupled MRF structure similar to the one shown in Fig. 4 is used. As discussed earlier, the decoupled MRF structure is able to extract precisely both the positive- and negative-sequence components of the fundamental-frequency voltage signals. The extracted positive sequence *d*-axis component is passed through a PI controller to generate an estimation of the angular speed of the component. The speed estimation, $\hat{\omega}$, is integrated to give the angular position $\hat{\theta}$, which is used in the transformation matrices for both positive and negative sequence reference frames.

Compared with DDSRF-PLL, the proposed MRF-based PLL method has a very straightforward implementation and almost identical performance. It can also be easily extended to include other harmonic components in the decoupling feedback structure if these components are large enough to degrade the PLL's performance.

A simulation was performed to verify the effectiveness of the proposed MRF-base PLL algorithm, in which the cutoff frequency of the low-pass filter was 60 Hz, and the parameters of the PI block were $K_p = 2.22$, and $K_i = 246.7$. Fig. 7 shows the responses of the MRF-PLL under various input voltage situations. Initially, the three-phase voltages were balanced and had a frequency of 48 Hz. At time $t = 0.5$ s, there was a step change in the utility frequency, which increased by 25% and became 60 Hz. The dynamics of the PLL under such a large step input can be clearly observed by looking at the estimated angular speed, which rapidly increased to the set value in less than one cycle. The effect of this step disturbance on the angular position theta was even more attenuated due to the low-pass filtering effect of the integrator.

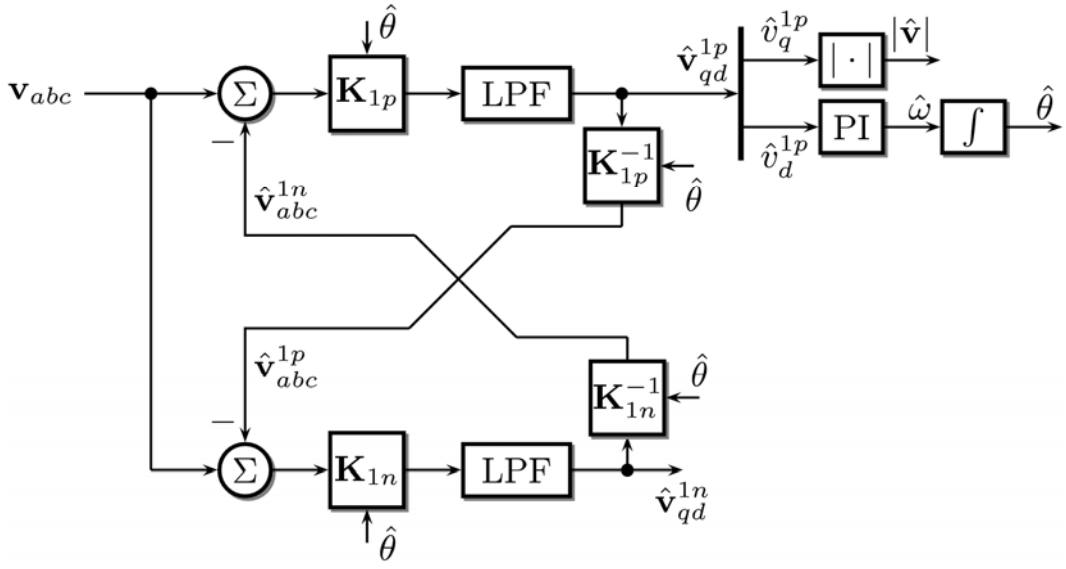

Fig. 6. Block diagram of the multiple reference frame based synchronization algorithm.

At time t = 0.15 s, the magnitude of phase a voltage was increased by 40%. This imbalance in magnitudes created negative sequence components in the source voltage. As can be seen in Fig. 7, the estimated electrical angular velocity only had a short period of transient process, then quickly settled down to its nominal value of 377 rad/s. No visible distortions in the angular position $\hat{\theta}$ is observed.

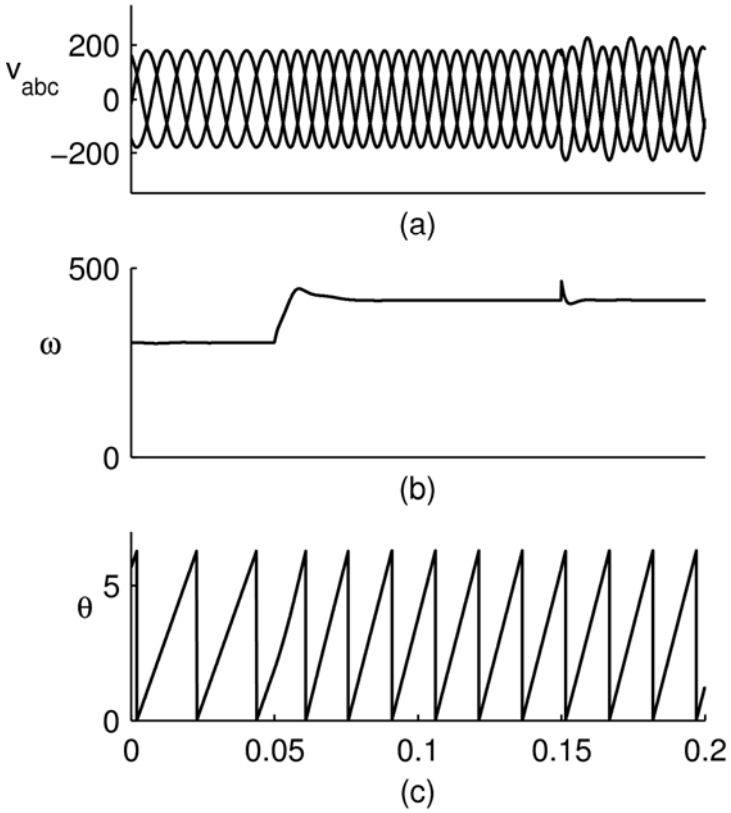

Fig. 7. Simulation results of the proposed MRF-based PLL algorithm. (a) Three-phase voltages (V); (b) Estimated electrical angular speed (rad/s); (c) Estimated phase angle (rad).

5. THE COMPLETE CONTROL ALGORITHM

The complete block diagram of the proposed rectifier control algorithm is shown in Fig. 8. The details of the two grayed blocks, MRF Compensation and MRF-PLL, have

already been described in previous sections. It can be observed that two parallel paths are used for the regulation of dc voltages and power factor. The reactive power is calculated directly from the three-phase voltages and currents with

$$Q = \frac{\sqrt{3}}{2}\left[v_{as}\left(i_{cs} - i_{bs}\right) + i_{as}\left(v_{bs} - v_{cs}\right)\right] \tag{13}$$

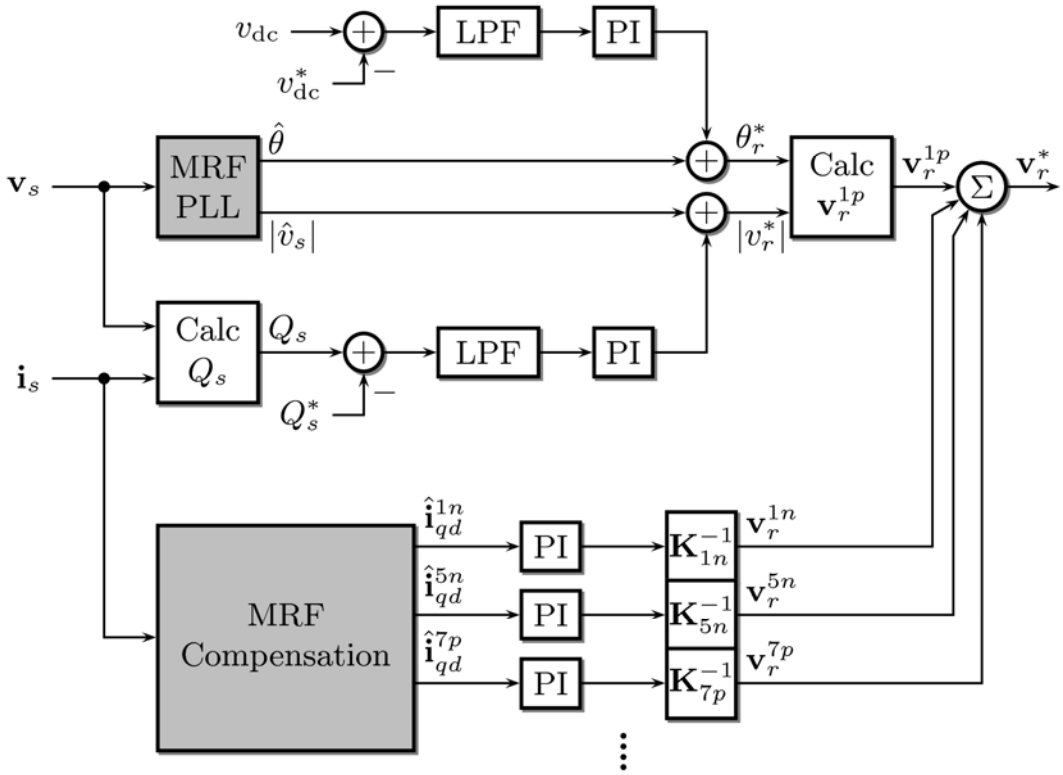

Fig. 8. Block diagram of the complete MRF-based active rectifier control.

The estimated *qd* quantities in each reference frame are passed through a PI block, then transformed back into the abc frame and added to the rectifier voltage references. This guarantees that in steady state all the harmonic components become zero. In this study, the negative sequence fundamental frequency component is also regulated to zero, which effectively maintains a balanced three-phase input currents even when the source

voltage is unbalanced. It should be pointed out, however, that other control strategies for unbalanced input can also be used by setting appropriate reference currents for the 1p and 1n current components [9].

6. EXPERIMENTAL RESULTS

6.1 Prototype Description

To experimentally verify the effectiveness of the proposed MRF-based technique, a 2 kW three-phase PWM boost-type rectifier prototype system was built in the laboratory. The system consists of a 1.2 mH three-phase input inductor, a rectifier bridge with six IGBTs (rated 600 V and 75 A), a dc link capacitor of 3900 μF, and a resistive dc load of 40 ohms. Hall effect voltage and current sensors were used to measure the output dc voltage (v_{dc}), input line-to-line voltages (v_{ab} and v_{bc}) and input currents (i_a and i_b).

The IGBTs were controlled by a fixed-point DSP (TMS320F2812 from Texas Instruments) with a clock frequency of 150 MHz. The switching and control frequency was set to 20 kHz. In each control cycle, the DSP samples the sensed signals and completes all the calculations needed to determine the switching states. In addition, two D/A channels were used so that internal variables can be displayed on an oscilloscope.

The proposed MRF-based rectifier control algorithm was implemented on the DSP. In addition to positive and negative synchronous reference frames 1p and 1n, three harmonic reference frames (2n, 5n, and 7p) were also used to target the 2nd, 5th, and 7th harmonics, respectively. A flag variable was used so that the harmonic/unbalance compensation function can be turned on or off while the system is running.

Although voltages from the electric power grid can become unbalanced and contain harmonics due to nonlinear loads, the amount of distortion cannot be controlled.

Therefore, to test the performance of the prototype system under various distorted conditions, a 5.25 kW three-phase programmable power supply (Elgar SW5250) was used as the input power source of the rectifier. The device can generate three-phase voltages of arbitrary phases and magnitudes, and the waveforms can be programmed using GPIB commands. It is thus very convenient to generate voltages with a controlled amount of imbalance and harmonics.

All the test results shown below were based on the following operating point: the line-to-line rms voltage of the power source is 120 V, the commanded dc link voltage is 280 V, and the rated load power is 1.96 kW.

6.2 Harmonic Compensation Test

In the first test, only harmonic components (5^{th} and 7^{th}) were intentionally added to the source voltages, and the three phases are balanced. Fig. 9 illustrates the test results recorded with an oscilloscope. Fig. 9 (a) shows the distorted input line-to-line voltages v_{ab} and v_{bc}, which contain 10% of 5^{th} harmonic and 5% of 7^{th} harmonic contents. It was mentioned in previous sections that if harmonic compensation algorithm is not used, even a small amount of low-order harmonic voltages can create highly distorted currents, which can be clearly seen in Fig. 9 (b). As expected, when the compensation function is turned on, the input currents (i_a and i_b) are much cleaner and become almost pure sinusoidal, as illustrated in Fig. 9 (c).

The spectra of the phase *a* current before and after the compensation are shown in Fig. 9 (d). As can be seen, the 2^{nd}, 5^{th} and 7^{th} harmonic components are completely canceled by the MRF algorithm. The THD of the current decreases from 19.5% to 1.7% when the compensation is in effect.

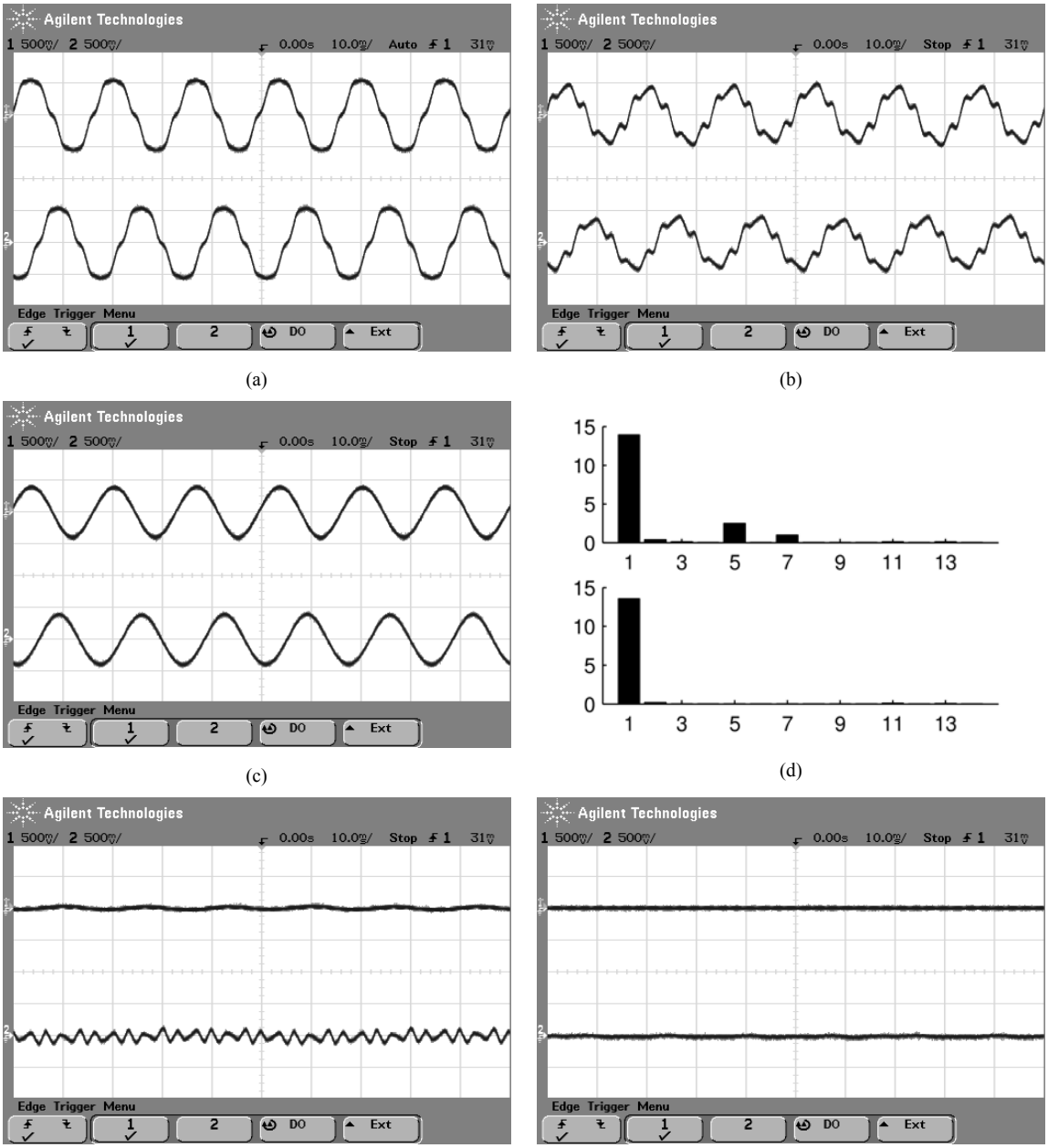

Fig. 9. Experimental results for test with balanced harmonic input voltages. (a) Line-to-line source voltages; (b) Input currents before compensation; (c) Input currents after compensation; (d) FFT results of phase *a* current before (top trace) and after (bottom trace) compensation; (e) 1*n* and harmonic components before compensation; (f) 1*n* and harmonic components after compensation.

In the proposed algorithm, the negative-sequence components and harmonic components in the source currents are separately extracted. Although these signals do not

physically exist and can only be obtained through calculations, they are important indicators of the degree of distortions in the currents. Through a two-channel D/A converter, the waveforms of i_a^{1n} and i_a^h are shown on a oscilloscope. Figs. 9 (e) and (f) shows these signals before and after the compensation is used. In Fig. 9 (e), only a very small negative sequence component (the top trace) can be seen because the three-phase source voltages are mainly balanced. However, the harmonic component (the bottom trace), which includes the sum of all harmonics, indicates that the input currents are highly distorted. In Fig. 9 (f), with the help of the MRF-based harmonic compensation method, both the negative-sequence and harmonic traces are very close to zero, indicating a relatively clean current waveform.

6.3 Unbalanced Harmonic Cases

Next, unbalanced conditions were added to the source voltages, which still contain the same amount of harmonics as in the previous test. In this case, the magnitude of the phase *a* voltage was decreased from 70 V to 50 V, which is a 28% reduction. The magnitudes of phase *b* and *c* voltages remained the same. The test results are depicted in Fig. 10.

To better illustrate this magnitude difference, the waveforms of line-to-line voltages v_{ab} and v_{bc} are placed on the same level in Fig. 10 (a). The effects of this unbalanced and harmonic voltages seriously degraded the performance of the rectifier control. As can be seen in Fig. 10 (b), not only did the input currents have large amount of 5^{th} and 7^{th} harmonics, other harmonic components (2^{nd}, 3^{rd}, 4^{th}, etc.) also appeared. Due to the unbalanced input voltage, the magnitude of i_a (top trace) was much lower than that of i_b (bottom trace).

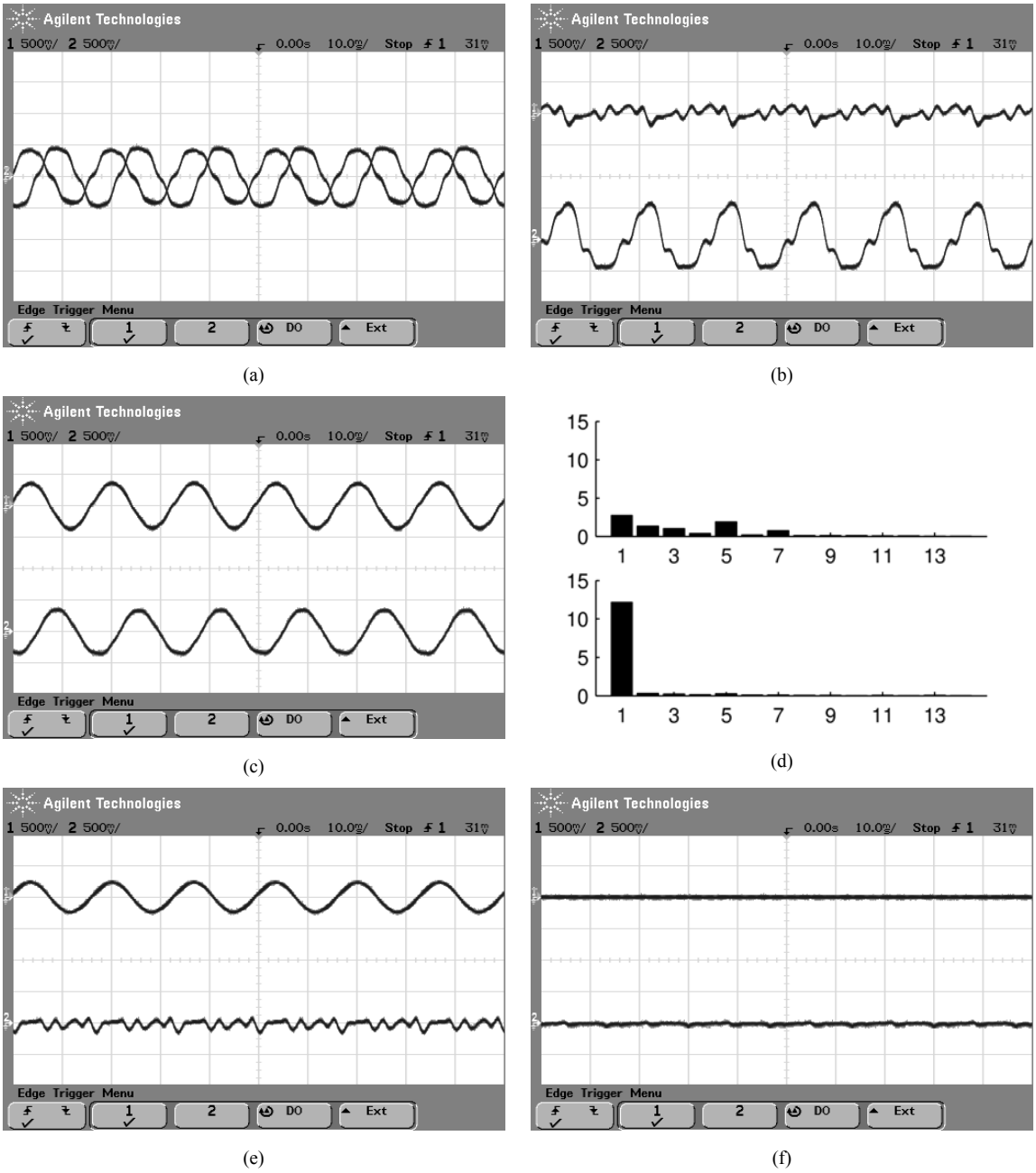

Fig. 10. Experimental results for test with unbalanced harmonic input voltages. (a) Line-to-line source voltages; (b) Input currents before compensation; (c) Input currents after compensation; (d) FFT results of phase *a* current before (top chart) and after (bottom chart) compensation; (e) 1*n* and harmonic components before compensation; (f) 1*n* and harmonic components after compensation.

Fig. 10 (c) shows the input current waveforms when the MRF-based compensation function is in effect. Apparently, the shapes of the waveforms are

significantly improved. FFT calculations showed that the three targeted harmonic components were adequately compensated, and the magnitude of the these harmonics were close to zero, as illustrated in Fig. 10 (d). The harmonic and imbalance compensation control achieved a great decrease in THD of the phase *a* current, which reduced from 98.7% to 4.4%. Figs. 10 (e) and (f) show the extracted negative-sequence and harmonic components in the input current. Without compensation, there exist a large amount of negative sequence current. Fig. 10 (f) clearly show that the compensation method can effectively balance the input currents.

It should be noted that because the harmonics are also unbalanced, they contain both positive and negative sequence components, and in theory two compensation channels should be used for each harmonic frequency to achieve completely compensation. However, in general the amount of non-typical harmonic components (positive 5^{th} and negative 7^{th}) are much smaller than those typical harmonic components (negative 5^{th} and positive 7^{th}). This fact justified the decision in the DSP program to only target the dominant typical harmonic components. On the other hand, if a specific harmonic component is particularly large, or a resonant condition is observed, a dedicated compensation channel should be added to the MRF-based algorithm.

6.4 Performance of MRF-PLL

It is noteworthy to look at the performance of the MRF-based PLL algorithm under unbalanced and harmonic input voltage conditions. Fig. 11 depicts waveforms of the estimated *q*-axis voltage in 1*p* reference frame (whose absolute value is equal to the magnitude of the input voltage) and the estimated phase angle. These were both internal variables in the DSP algorithm and brought out using D/A channels. The voltages used

for this experiment contain a large amount of 5th and 7th harmonics; they also contain a significant amount of negative sequence components, which normally have a large negative impact on the identification of voltage phase information.

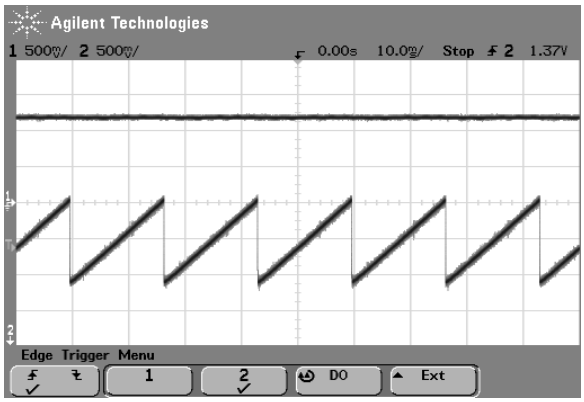

Fig. 11. Experimental results of the MRF-PLL algorithm under distorted input conditions. Top trace: estimated q-axis values in 1p reference frame; Bottom trace: estimated phase angle.

Fig. 11 shows that the estimated phase angle and magnitude have very little ripple. This result is expected since the MRF-PLL decouples the interaction between positive and negative sequence components of the fundamental-frequency source voltage. Due to the low-pass filtering effect of the integrator, the harmonics have almost no visible impact on the phase angles. Some harmonic ripple may still appear in the magnitude waveform, even though they are attenuated by the LPF.

6.5 Dynamic Response Test

The fast dynamic response feature of the proposed MRF-based compensation algorithm can be appreciated by investigating its transient behavior. Fig. 12 depicts waveforms of the input currents (i_a and i_b) when there was a sudden turn-on of the algorithm. Before compensation, the unbalanced and distorted nature of the currents can

be clearly seen. When the algorithm was turned on at time t = 200 ms, i_a and i_b became balanced and free of low-order harmonics almost instantly, only after a short period of transient process.

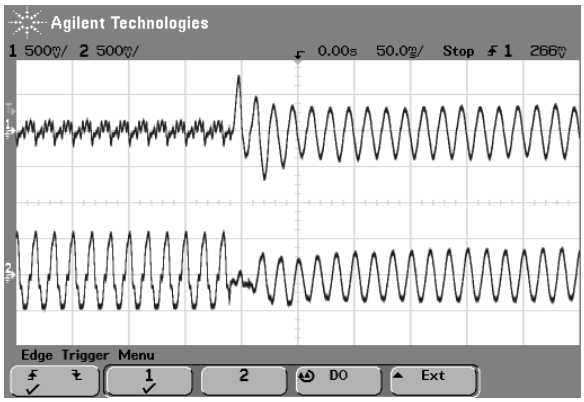

Fig. 12. Experimental results of the dynamic performance test. Compensation algorithm is turned on at time t = 200 ms. Top trace: phase *a* current; Bottom trace: phase *b* current.

7. CONCLUSIONS

A multiple reference frame based harmonic compensation algorithm for grid-connected three-phase power converter applications has been presented in this paper. A decoupled multiple reference frame architecture is proposed to eliminate interferences between components of different frequencies, which enables the selective compensation of dominant harmonics currents. Furthermore, a MRF-PLL technique was set forth to precisely track the frequency and phase information of the utility system. The presence of imbalance or distortion in the source voltages does not degrade the performance of the phase-locked loop operation. The decoupled structure can cleanly extract the fundamental positive sequence component without sacrificing good dynamic performance. A complete experimental evaluation based on a three-phase rectifier system demonstrated that the

proposed technique can yield fast and accurate operation. Balanced sinusoidal input currents can be achieved even under severe unbalanced and harmonic input conditions.

8. REFERENCES

[1] P. Pejovi and Z. Janda, "An analysis of three-phase low-harmonic rectifiers applying the third-harmonic current injection," *IEEE Trans. Power Electron.*, vol. 14, pp. 397-407, May 1999.

[2] D. Alexa, A. Sirbu, and A. Lazar, "Three-phase rectifier with near sinusoidal input currents and capacitors connected on the ac side," *IEEE Trans. Ind. Electron.*, vol. 53, pp. 1612-1620, Oct. 2006.

[3] B. M. Saied and H. I. Zynal, "Minimizing current distortion of a three-phase bridge rectifier based on line injection technique," *IEEE Trans. Power Electron.*, vol. 21, pp. 1754-1761, Nov. 2006.

[4] H. Fujita and H. Akagi, "An approach to harmonic current-free AC/DC power conversion for large industrial loads: The integration of a series active filter with a double-series diode rectifier," *IEEE Trans. Ind. Applicat.*, vol. 33, Sep./Oct. 1997.

[5] S. Kwak and H. A. Toliyat, "Design and rating comparisons of PWM voltage source rectifiers and active power filters for AC drives with unity power factor," *IEEE Trans. Power Electron.*, vol. 20, Sep. 2005.

[6] L. Moran, P. D. Ziogas, and G. Joos, "Design aspects of synchronous PWM rectifier-inverter system under unbalanced input voltage conditions," *IEEE Trans. Ind. Applicat.*, vol. 28, pp. 1286-1293, Nov./Dec. 1992.

[7] D. Vincenti and H. Jin, "A three-phase regulated PWM rectifier with on-line feedforward input unbalance correction," *IEEE Trans. Ind. Electron.*, vol. 41, pp. 526-532, Oct. 1994.

[8] A. V. Stankovic and T. A. Lipo, "A novel control method for input output harmonic elimination of the PWM boost type rectifier under unbalanced operating conditions," *IEEE Trans. Power Electron.*, vol. 16, pp. 603-611, Sep. 2001.

[9] H. Song and K. Nam, "Dual current control scheme for PWM converter under unbalanced input voltage conditions," *IEEE Trans. Ind. Electron.*, vol. 46, pp. 953-959, Oct. 1999.

[10] P. Rioual, H. Pouliquen, and J. P. Louis, "Regulation of a PWM rectifier in the unbalanced network state using a generalized model," *IEEE Trans. Power Electron.*, vol. 11, pp. 495-502, May 1996.

[11] J. Wu, F. C. Lee, and D. Boroyevich, "Elimination of low-frequency harmonics caused by PWM in a three-phase soft-switched boost rectifier," *IEEE Trans. Ind. Applicat.*, vol. 38, pp. 483-489, Mar./Apr. 2002.

[12] P. Xiao, K. A. Corzine and G. K. Venayagamoorthy, "Cancellation Predictive Control for Three-Phase PWM Rectifiers under Harmonic and Unbalanced Input Conditions," *Proceedings of the Conference of the IEEE Industrial Electronics Society*, 2006, pp. 1816-1821.

[13] M. J. Newman, D. N. Zmood, and D. G. Holmes, "Stationary Frame Harmonic Reference Generation for Active Filter Systems," *IEEE Trans. Ind. Applicat.*, vol. 38, pp. 1591-1599, Nov./Dec. 2002.

[14] P. Mattavelli, "Synchronous-frame harmonic control for high-performance AC power supplies," *IEEE Trans. Ind. Applicat.*, vol. 37, pp. 864-872, May/Jun. 2001.

[15] Y. Sato, T. Ishizuka, K. Nezu, and T. Kataoka, "A new control strategy for voltage-type PWM rectifiers to realize zero steady-state control error in input current," *IEEE Trans.* Ind. *Applicat.*, vol. 34, pp. 480-486, May/Jun. 1998.

[16] D. N. Zmood and D. G. Holmes, "Stationary frame current regulation of PWM inverters with zero steady-state error," *IEEE Trans. Power Electron.*, vol. 18, pp. 814-822, May 2003.

[17] D. N. Zmood, D. G. Holmes, and G. H. Bode, "Frequency-domain analysis of three-phase linear current regulators," *IEEE Trans. Ind. Applicat.*, vol. 37, pp. 601-610, Mar./Apr. 2001.

[18] X. Yuan, W. Merk, H. Stemmler, and J. Allmeling, "Stationary frame generalized integrators for current control of active power filters with zero steady-state error for current harmonics of concern under unbalanced and distorted conditions," *IEEE Trans. Ind. Applicat.*, vol. 38, pp. 523-532, Mar./Apr. 2001.

[19] S. Fukuda and R. Imamura, "Application of a sinusoidal internal model to current control of three-phase utility-interface converters," *IEEE Trans. Ind. Electron.*, vol. 52, pp. 420-426, Apr. 2005.

[20] V. Blasko, "A novel method for selective harmonic elimination in power electronic equipment," *IEEE Trans. Power Electron.*, vol. 22, pp. 223-228, Jan. 2007.

[21] C. D. Schauder and S. A. Moran, "Multiple reference frame controller for active filters and power line conditioners," U.S. patent 5,309,353, May 1994.

[22] S. J. Lee and S. K. Sul, "A harmonic reference frame based current controller for active filter," in *Proc. IEEE Applied Power Electronics Conf*., 2000, pp. 1073-1078.

[23] A. Jin, H. Li, and S. Li, "A flexible input currents control strategy for three-phase pfc rectifier under unbalanced system," in *Proc. IEEE Industrial Electronics and Applications Conf*., 2006, pp. 1-6.

[24] P. C. Krause, "Method of multiple reference frames applied to the analysis of symmetrical induction machinery," *IEEE Trans. Power Apparatus and Systems*, vol. pas-87, Jan. 1968.

[25] S. D. Sudhoff, "Multiple reference frame analysis of an unsymmetrical induction machine," *IEEE Trans. Energy Convers*., vol. 8, pp. 425-432, Sep. 1993.

[26] S. D. Sudhoff, "Multiple reference frame analysis of a multistack variable-reluctance stepper motor," *IEEE Trans. Energy Convers*., vol. 8, pp. 418-424, Sep. 1993.

[27] P. L. Chapman, S. D. Sudhoff, and C. A. Whitecomb, "Multiple reference frame analysis of nonsinusoidal brushless DC drives," *IEEE Trans. Energy Convers.*, vol. 14, no. 3, pp. 440–446, Sep. 1999.

[28] S. M. Cruz and A. J. Cardoso, "Multiple reference frames theory: a new method for the diagnosis of stator faults in three-phase induction motors," *IEEE Trans. Energy Convers*., vol. 20, pp. 611-619, Sep. 2005.

[29] P. L. Chapman and S. D. Sudhoff, "A multiple reference frame synchronous estimator/regulator," IEEE *Trans. Energy Convers.*, vol. 15, pp. 197-202, Jun. 2000.

[30] V. Kaura and V. Blasco, "Operation of a phase locked loop system under distorted utility conditions," *IEEE Trans. Ind. Applicat.*, vol. 33, pp. 58–63, Jan./Feb. 1997.

[31] P. Rodriguez, J. Pou, J. Bergas, et al., “Decoupled double synchronous reference frame pll for power converters control,” *IEEE Trans. Power Electron.*, vol. 22, pp. 584-592, Mar. 2007.

PAPER III

Impedance Measurement Technique for Power Electronic Systems Based on Recurrent Neural Networks

Peng* Xiao, *Ganesh K. Venayagamoorthy, and Keith A. Corzine

Real-Time Power and Intelligent Systems Laboratory

Department of Electrical and Computer Engineering

University of Missouri-Rolla, Rolla, MO, 65401 USA

pxfx7@umr.edu, gkumar@ieee.org and keith@corzine.net

ABSTRACT

When designing and building power systems that contain power electronic switching sources and loads, system integrators must consider the frequency-dependent impedance characteristics at an interface to ensure system stability. Stability criteria have been developed in terms of source and load impedance for both dc and ac systems and it is often necessary to measure system impedance through experiments. Traditional injection-based impedance measurement techniques require multiple online tests which lead to many disadvantages. The impedance identification method proposed in this paper greatly reduces online test time by modeling the system with recurrent neural networks. The recurrent networks are trained with measured signals from the system with only one stimulus injection per frequency decade. The measurement and identification processes for dc and three-phase ac interfaces are developed. Simulation and laboratory tests demonstrate the effectiveness of this new technique.

Keywords

impedance measurement, recurrent neural network, stability analysis

1. INTRODUCTION

Stability analysis in power electronics based distributed power systems is a more crucial task than in conventional power systems due to the nearly ideal control capability of many modern power converters. The excellent load regulation capability of a converter is a desirable feature in many applications, but it also makes the converter a constant-power load device, which is a potential cause of negative impedance instability [1].

For small-signal stability analysis, most research focuses on the impedance/admittance method that involves examining the Nyquist contour of the product of the source impedance and load admittance in a dc system [2]. In recent years, based on the impedance/admittance method, a variety of stability criteria and design approaches for both dc and ac systems have been proposed [3-4].

In the design, integration and analysis of distributed power systems, it is often necessary to obtain the small-signal impedance/admittance characteristics of an existing power electronic component or subsystem at a given operating point. To get the frequency-dependent characteristics by experiment, periodic voltage or current perturbations are usually injected to the system while it is under operational power. Measurements of the perturbed system are then taken and processed to determine the impedance at a specific frequency. Several methods have been proposed for impedance measurement in high-power ac systems, including utilization of three-phase bridge converters, wound-rotor induction machines and three-phase chopper circuit [5-6]. An impedance measurement technique utilizing a line-to-line current injection chopper circuit was recently proposed [7], which has a simple structure and is easier to implement compared with other methods.

A common problem of these impedance measurement techniques is that they require injection of perturbation signals to the system one frequency at a time. To obtain the impedance characteristics over a wide frequency range for stability analysis, multiple tests must be repeatedly performed. During each test, a perturbation signal of a specific frequency is injected into the system, and the voltages and currents are measured and recorded. When tests for all frequencies are finished, the recorded data is processed to calculate the impedance value at each frequency. The main disadvantages of this procedure include: (i) It takes a long online time to complete the injections for all frequencies; (ii) The operating point of the system may vary during the prolonged test procedure, which can lead to inconsistency in the measured system impedance characteristics; (iii) If the impedances at additional frequencies are needed, new tests must be performed on the system, which may cause interruption to the normal operation of the system.

In this paper, a different approach is taken to identify the impedance characteristics of a dc or three-phase ac system. Instead of measuring system impedance at one specific frequency each time, the proposed method requires only one injection and measurement process. The recorded data is used not to directly calculate impedances, but to build a model of the system at the specified operating point by training a recurrent neural network (RNN). The trained RNN is then used to obtain the impedance characteristics. Results from both simulation and laboratory tests show that the proposed method is capable of accurately identifying impedances of both dc and three-phase ac systems.

2. IMPEDANCE MEASUREMENT FOR STABILITY ANALYSIS

The analysis of small-signal stability around steady states of a power electronic system is important for both control design and component integration. In the design stage, if the mathematical model of the system is known, it can be used to extract the impedance characteristics of the system. In addition, models of different system components can be connected together to simulate their behavior under different operating conditions, and linearization tools are usually available to determine the state-space matrices of the system. The situation is different in the component integration stage, when the hardware components are connected together to form a system. In this case, the detailed models of the components are often not available, especially when the components are designed and manufactured by different vendors. To evaluate the stability of the integrated system, measurements and tests are necessary to obtain the impedance information of each component.

The injection-based impedance measurement techniques utilize small voltage or current signals to perturb the system under study, while it is operating in steady state. Various injection devices have been proposed. For low-power systems, power amplifiers can be used. For high-power systems, different configurations of chopper circuits are often used, in which switching devices are turned on and off to provide a varying impedance branch that creates the perturbations.

Fig. 1 shows the shunt injection diagram for dc systems. The system is divided into two parts, designated as source and load, although the actual power flow can be either from the load to the source or from the source to the load. The injection device is connected at their common interface. In the shunt injection system, a current signal of a

specific frequency is injected into the system at a steady-state operating point. The dc voltage at the interface, together with the load and source currents, are measured. The waveforms of these signals are recorded. Fourier transform is then used to process these signals and determine the magnitudes and phase angles of the components at the injection frequency. The small signal impedances of the load and source can then be calculated with

$$Z_s(f_i) = -\frac{V(f_i)}{I_s(f_i)} \qquad Z_l(f_i) = \frac{V(f_i)}{I_l(f_i)} \tag{1}$$

where f_i is the injection frequency, V, I_s and I_l are complex numbers obtained from Fourier transform of the dc voltage, source current, and load current signals. This single injection test gives the impedance information of the system at a single frequency f_i. To obtain impedances at other frequencies, the same test procedure is be repeated, each time with a different injection frequency.

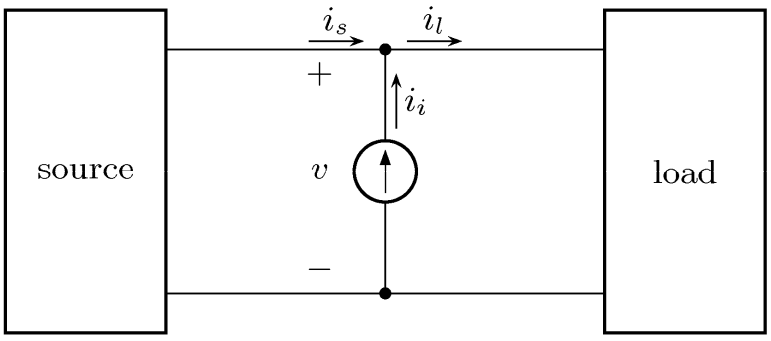

Fig. 1. Impedance measurement in dc systems.

The impedance measurement test for three-phase ac systems is more complicated. As shown in Fig. 2, the shunt injection requires a three-phase current source and measurement of nine signals. Also, the impedance information for the source and load is

represented by a 3 by 3 matrix. For three-phase balanced systems, reference frame transformation theory provides a convenient way to study the impedance characteristics. In the synchronous reference frame, the impedance and admittance take matrix forms

$$\begin{bmatrix} V_q \\ V_d \end{bmatrix} = \mathbf{Z} \begin{bmatrix} I_q \\ I_d \end{bmatrix} \qquad \begin{bmatrix} I_q \\ I_d \end{bmatrix} = \mathbf{Y} \begin{bmatrix} V_q \\ V_d \end{bmatrix} \tag{2}$$

where

$$\mathbf{Z} = \begin{bmatrix} Z_{qq} & Z_{qd} \\ Z_{dq} & Z_{dd} \end{bmatrix} \qquad \mathbf{Y} = \mathbf{Z}^{-1} = \begin{bmatrix} Y_{qq} & Y_{qd} \\ Y_{dq} & Y_{dd} \end{bmatrix} \tag{3}$$

To determine the four impedance entries in the matrix, two sets of injection signals are needed at each frequency. This actually doubles the number of tests needed to identify the system impedance characteristics over a wide frequency range.

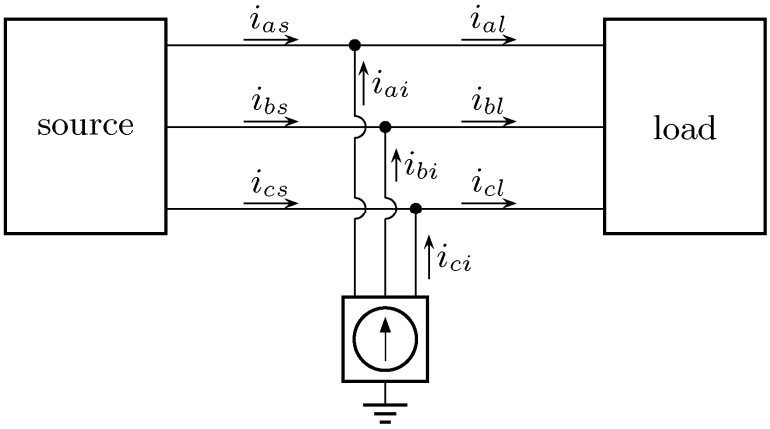

Fig. 2. Impedance measurement in three-phase ac systems.

3. RNN-BASED IMPEDANCE IDENTIFICATION METHOD

The key point of the proposed method is the modeling of a dynamic system under study. If a model can be built to accurately produce the small-signal time-domain

responses of the system to all types of inputs, then it also has the ability to produce the frequency-domain characteristics of the system. For an existing hardware system, the internal device parameters are often unavailable, thus it is impractical to build the model based on knowledge of the device's internal structure and control algorithms. Instead, the model can be created based on the input and output signals of the device.

3.1 Recurrent neural network as a modeling tool

For dynamic systems, a recurrent neural network has been demonstrated to be an effective modeling tool in many applications. Unlike the widely-used multilayer feedforward neural networks that can only establish static mapping relationship between inputs and outputs, RNNs contain internal feedback loops and states. The outputs of RNNs are functions of internal states as well as the inputs, just as they are in dynamic systems. The feedback mechanism provides a memory to the recurrent networks so that they are capable of modeling systems with internal dynamics. In this study, the Elman RNN topology is chosen for the modeling.

Fig. 3 shows a simplified diagram of a two-layer Elman recurrent network structure. For a network with l inputs, m hidden neurons, and n outputs, the hidden layer equations are

$$s_k(t) = \sum_{i=1}^{l} w_{ik}^{(1)} x_i(t) + \sum_{j=1}^{m} w_{jk}^{(2)} d_j(t-1) \tag{4}$$

where

$$d_k(t) = \mathrm{sgm}(s_k(k)) \tag{5}$$

$\boldsymbol{x}(t)$ is the input vector, $\boldsymbol{w}^{(1)}$ is the weight matrix associated with the inputs and hidden neurons, and $\boldsymbol{w}^{(2)}$ is the weight matrix associated with the states and hidden neurons.

The outputs of the network are determined by

$$y_k(t) = \sum_{i=1}^{m} w_{ik}^{(3)} d_i(t) \tag{6}$$

where $\boldsymbol{w}^{(3)}$ is the weight matrix associated with the hidden neurons and the outputs.

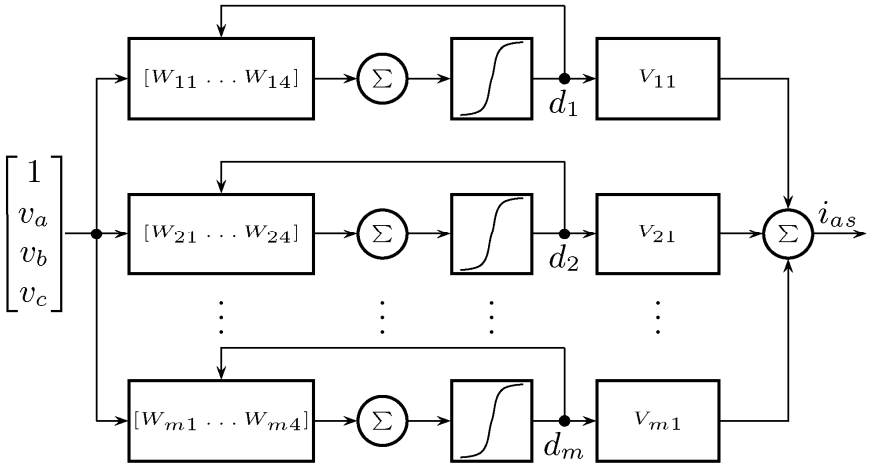

Fig. 3. Topology of the Elman recurrent network.

Past research has demonstrated the ability of the RNN to learn system dynamics and provide efficient predictions, and it has found application in many areas such as wind speed and power forecasting [8], design of a power system stabilizers [9], induction motor speed estimation [10], and prediction of elephant migration [11].

3.2 Modeling with RNN

To model a dynamic system with RNN, the network must be trained with measured data so that it learns the behavior of the system. It should be noted that the purpose of the training is not to obtain a complete model of the complex nonlinear power electronic system. Instead, throughout the test, the system is running at a specific steady-state operating point. Small variations of voltage or current are added to the system to

create perturbations. The RNN is then used to model the behavior of the system responding to small signal inputs.

The measured signals are voltage and current waveforms at the interface of the source and load. These waveforms are used as training data for the input and target output of the RNN. During the training process, input data are fed to the network to calculate the output, and the internal weight parameters of the RNN are adjusted based on the output error. Several RNN training algorithms are available. Both back-propagation and particle swarm optimization algorithms [12] are used in this study.

3.3 Random PWM signal injection

Training of the RNN requires measurement data of a perturbed system, thus injection of perturbation signals is still necessary in the proposed method. For the shunt injection, chopper circuits proposed in [7] are used to handle the high voltage and power of the tested system. Fig. 4 shows the circuit as being used for line-to-line current injection in a three-phase ac system. The circuit contains a bi-directional switch that controls the branch's impedance, which in turn causes variations in the branch current. A properly designed switching pattern can thus introduce a perturbation current signal into the system. A fixed-frequency fixed-duty-cycle PWM switching scheme was used in [7] to generate a perturbation signal of a specific frequency.

For the RNN to learn the dynamic behavior of the system, the spectrum of the perturbation signal must cover a wide frequency range. A random PWM signal with limited bandwidth is used in this study, which can be generated by a PWM switching scheme with a random duty cycle and random switching frequency. In each PWM cycle, the switching frequency is randomly chosen between two bounds, $f_{\min}$ and $f_{\max}$, which are

determined according to the frequency range of interest. Fig. 5 shows the spectrum of such a switching signal, with f_{min} = 1 kHz and f_{max} = 5 kHz. It can be seen that the signal has a relatively even magnitude at frequencies below 3 kHz. At frequencies above 3 kHz, the magnitude decreases with a slope between 20 dB/decade and 40 dB/decade.

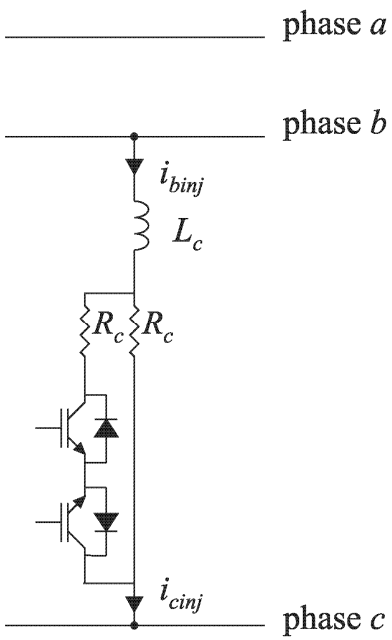

Fig. 4. Chopper circuit shown in three-phase system injection.

During the period when the system is being perturbed by a random PWM switching circuit, the voltage and current signals of the source and load are measured, filtered, and recorded. For a dc system, the recorded data is normalized and used directly to train the RNN. Either the voltage or the current signal can be used as the input, and the other signal is used as the target output. For a three-phase ac system, the measured signals are first transformed into the synchronous reference frame so that the fundamental components become dc signals. After normalization, the data is then used for RNN training.

The training process of the RNN involves repeatedly feeding the network with the input data, calculating the outputs, and comparing the calculated outputs with the target outputs. The network weights are modified in each epoch to minimize the error. The training stops when the error is below a certain threshold value.

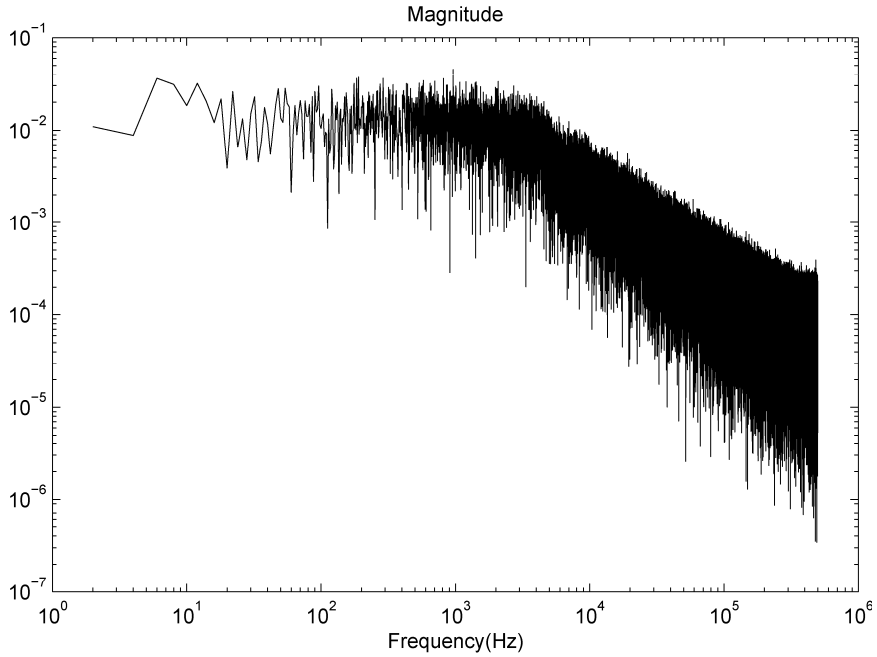

Fig. 5. Spectrum of a random PWM signal.

A well-trained RNN can produce correct outputs even when the inputs are different from its training data. It is this generalization capability of RNNs that makes them suitable for impedance characteristics extraction. The trained RNN can be seen as an accurate small-signal model of the system, and tests can be performed on the RNN instead of on the real system to obtain the impedance information.

3.4 Identification process for dc systems

For a dc system, to determine the impedance value at a frequency f_i, a sinusoidal signal of frequency f_i is fed to the trained RNN to produce the output. The input and output signals are then processed with Fourier transform to determine their magnitudes and phase angles at the injection frequency. The impedance and admittance of the system at f_i can be calculated with (1). Fig. 6 depicts the whole procedure with a flow chart.

3.5 Identification process for three-phase ac systems

For a three-phase ac system, if the RNN is trained with currents as inputs and voltages as outputs, then it is relatively easier to calculate the impedance matrix. For each frequency f_i, there are four impedance values to be determined and two steps are needed.

In the first step, a sinusoidal signal of frequency f_i is fed to the trained RNN as i_q, while the input signal i_d is set to a zero vector. The RNN output voltages v_q and v_d are then calculated with (4)-(6). According to (2), two impedance entries can be determined by

$$Z_{qq}(f_i) = \frac{V_q(f_i)}{I_q(f_i)} \qquad Z_{dq}(f_i) = \frac{V_d(f_i)}{I_q(f_i)} \tag{7}$$

where V_q, V_d and I_q are the complex results from Fourier transform of v_q, v_d and i_q, respectively. The second step is similar to the first one except that the sinusoidal signal is fed to the RNN as i_d, while i_q is set to zero. The other two impedance entries can be determined by

$$Z_{dd}(f_i) = \frac{V_d(f_i)}{I_d(f_i)} \qquad Z_{qd}(f_i) = \frac{V_q(f_i)}{I_d(f_i)} \tag{8}$$

Fig. 7 shows a flowchart of the proposed impedance measurement procedure for three-phase ac systems. It can be seen that the online part of the procedure only includes the injection of the random PWM signal and data measurement, and the rest of the process only requires offline training and calculations.

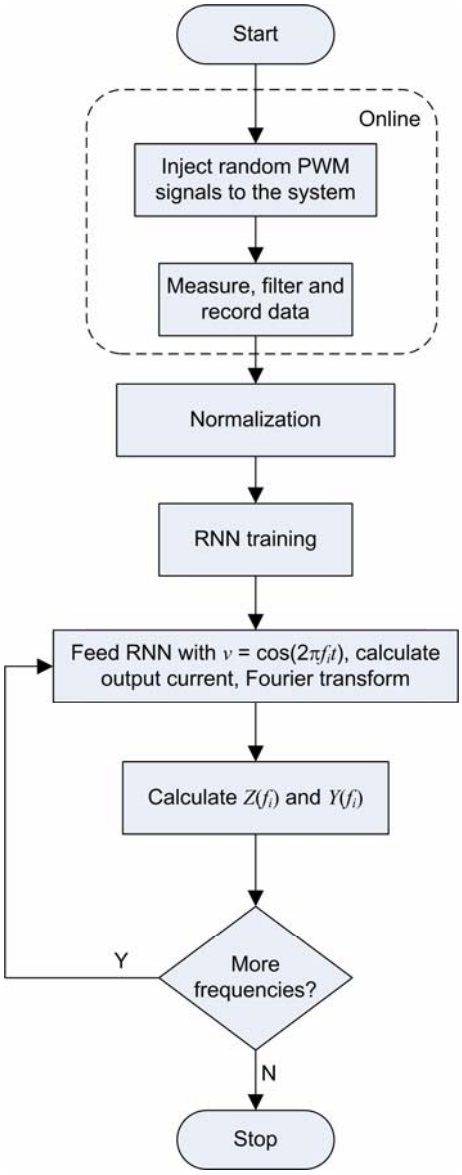

Fig. 6. Flow chart of the proposed impedance measurement procedure for dc systems.

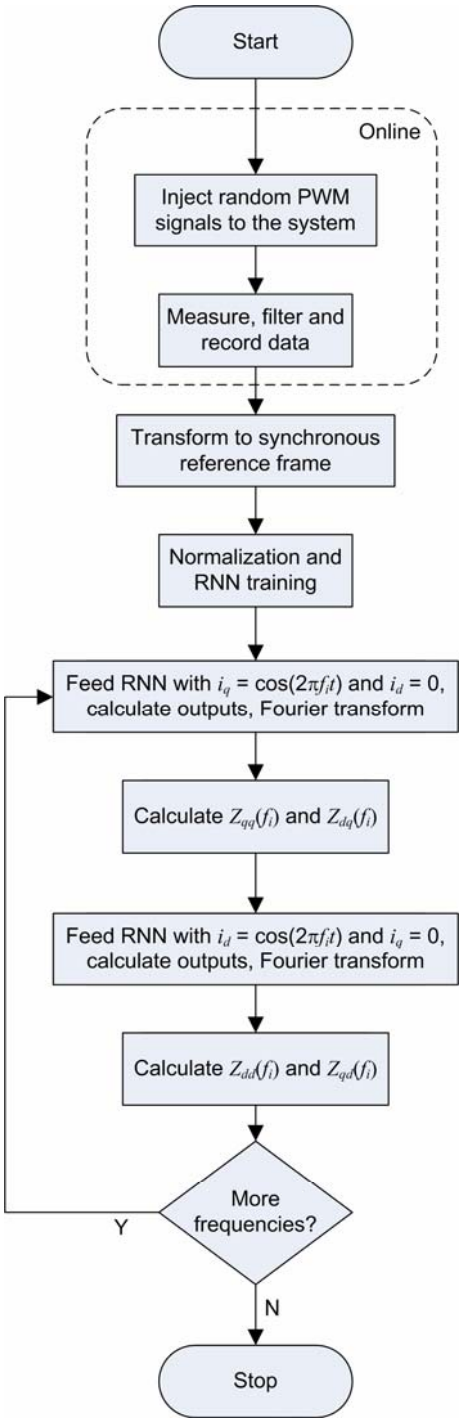

Fig. 7. Flow chart of the proposed impedance measurement procedure for three-phase ac systems.

4. SIMULATION RESULTS

The proposed impedance measurement technique was verified with simulation results of both dc and three-phase ac systems.

4.1 Test results in dc systems

A 3.7 kW variable-speed motor drive system is used for the dc test, and its diagram is shown in Fig. 8. The example system consists of a three-phase active rectifier, 300 V dc link, a three-phase inverter, and a 5 hp induction motor. Input and output filters are used to reduce the PWM switching noises.

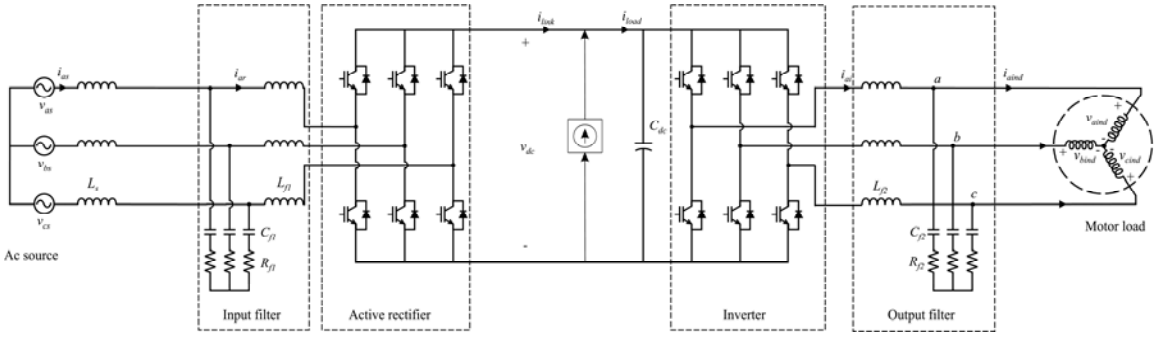

Fig. 8. Test system for dc impedance measurement.

The dc link interface of a rectifier-inverter-induction motor system is used for the dc signal injection. The location of the injection device is shown in Fig. 8, where the current source on the dc link represents the chopper circuit as shown in Fig. 4. To measure the impedance of the subsystem to the right of the injection device, both v_{dc} and i_{load} are measured and saved. The frequency range of interest is from 10 Hz to 1 kHz, and the frequency bounds of the random PWM signal is set to be 400 Hz and 1 kHz. The measured signals are filtered to avoid aliasing, and sampled at a frequency of 10 kHz. The data is then normalized to be within the range from -1 to 1. An Elman RNN is

trained with the voltage data as input and current data as output. The extracted impedance characteristics are shown in Fig. 9. The actual impedance curves are obtained based on the linearized state-space matrix in a simulation model of the system. As can be seen, a very close match between the measured and actual values is achieved.

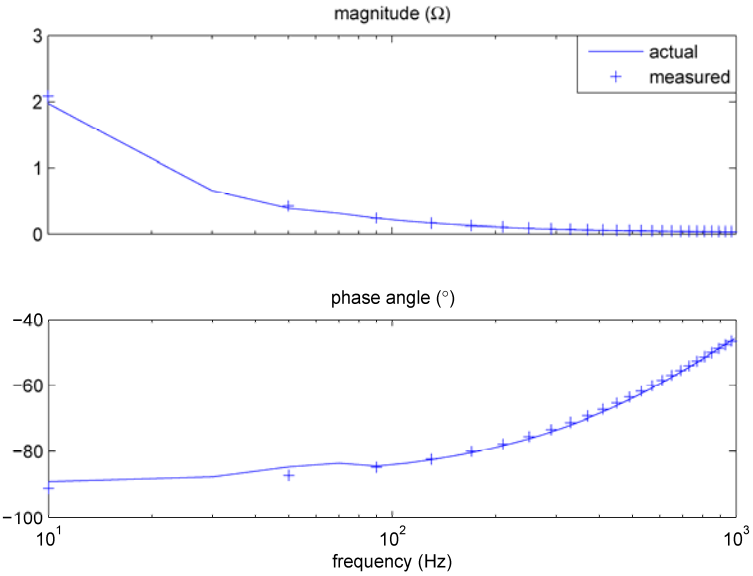

Fig. 9. Jacobian and RNN extracted impedances of the dc subsystem.

4.2 Test results in ac systems

The ac test system includes a salient-pole synchronous generator feeding an *R*-*L* load (R = 27.29 Ω, L = 19.9 mH). The chopper circuit is connected to the *b* and *c* phases of the generator terminals. The injection and data processing conditions are similar to those in the dc test, except that the *abc* signals are transformed into the synchronous reference frame before normalization. An Elman RNN is used for the training, where the inputs are the currents and the outputs are the voltages.

For a symmetric three-phase *R-L* load, its impedance matrix in the synchronous reference frame can be expressed as

$$\mathbf{Z}_{RL}(\omega)=\begin{bmatrix} R+j\omega L & \omega_e L \\ -\omega_e L & R+j\omega L \end{bmatrix} \tag{9}$$

where ω_e is the speed of the synchronous reference frame. Figs. 10 and 11 clearly show the agreement between (9) and the measured impedance characteristics.

Fig. 12 shows the measured magnitude curves of Z_{qq} and Z_{dd} of the synchronous generator. The impedances identified with the proposed method are very close to the actual values. The *q*- and *d*-axis impedances are different because of rotor saliency of the generator.

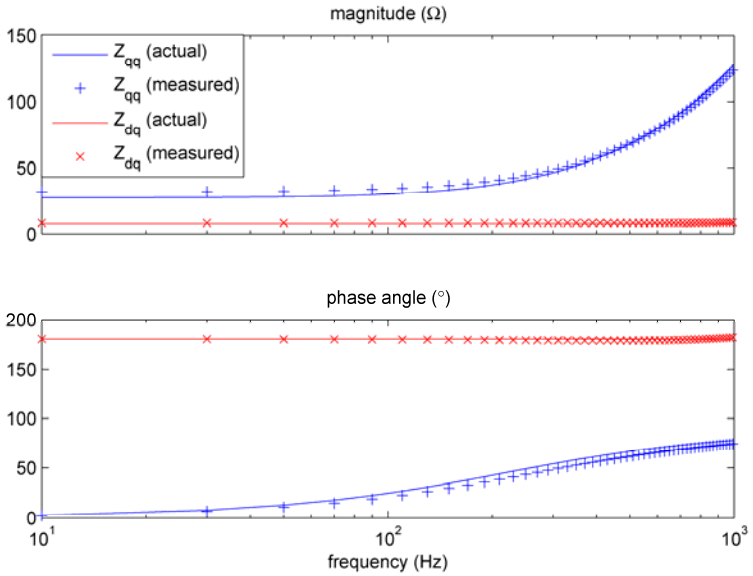

Fig. 10. Impedances Zqq and Zdq of a three-phase RL load.

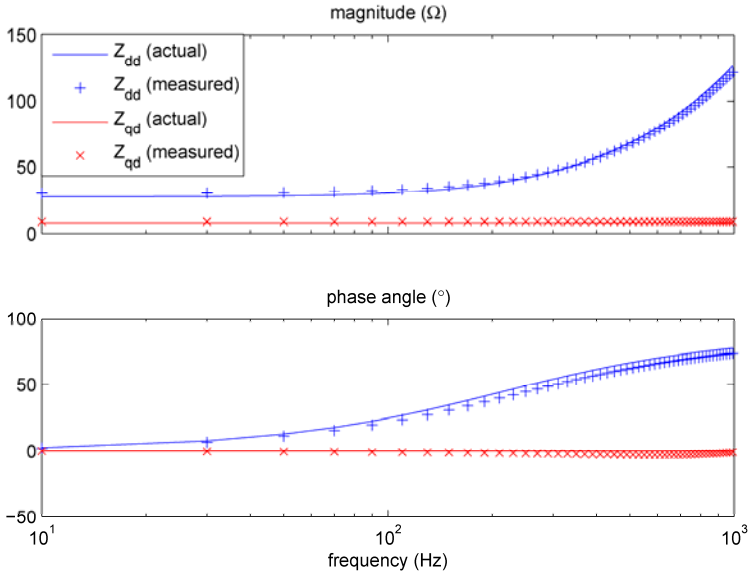

Fig. 11. Impedances Zdd and Zqd of a three-phase RL load.

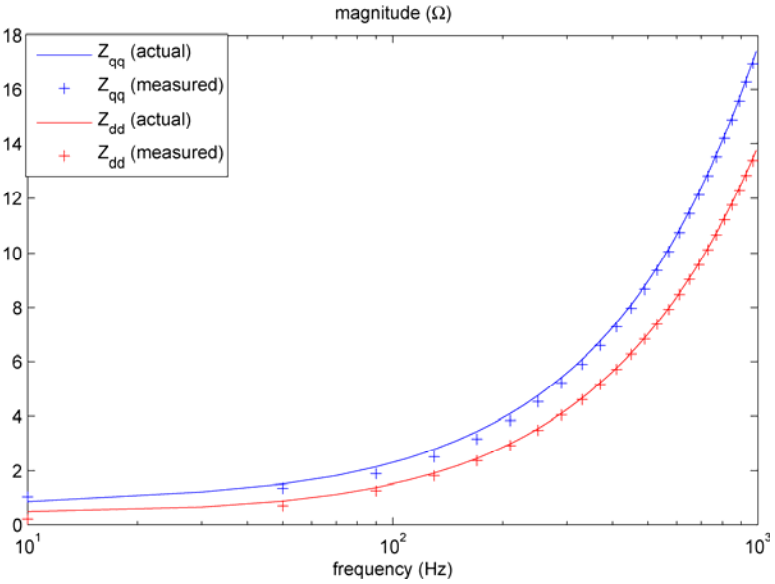

Fig. 12. Impedances Zqq and Zdd of a three-phase synchronous generator.

4.3 Evaluation of impedance accuracy

The accuracy of the proposed impedance identification method depends on several factors. Firstly, signal measurement errors have a large impact on the RNN

training data because the small perturbation signals are usually added to very large steady-state currents and voltages. Secondly, the RNNs also contribute to impedance inaccuracies. The number of hidden neurons is directly related to the modeling capabilities of a network. Generally more neurons are needed for the RNN to accurately model systems with complex dynamics. Finally, since RNNs contain internal states, their initial values also affect the accuracy of the model. Their effects can be reduced by discarding the first portion of the input and output data in the identification process.

5. EXPERIMENTAL RESULTS

The further verify the effectiveness of the proposed impedance identification method, a laboratory prototype system similar to the one shown in Fig. 8 was built. The parameters of the passive components in the system are listed in Table I.

Table I. Component parameters of the experimental system.

L_s = 0.4 mH	r_s = 0.5 ohms
L_{f1} = 1.8 mH	L_{f2} = 1.2 mH
C_{f1} = 5 μF	C_{f2} = 5 μF
R_{f1} = 10.4 ohms	R_{f2} = 10.4 ohms
C_{dc} = 3900 μF	

A practical concern arises when the proposed method is applied in a real-world system. Although the RNN model can be trained with recorded voltages and currents when random PWM signals are injected, it is difficult to choose the sampling rate of the recording device if the frequency range of interest is wide. On the one hand, high sampling rate is desired to capture system responses to high frequency signals. On the

other hand, large number of training data points will significantly slow down the RNN training process if the sampling rate is high. It should be noted that different frequency bands have different requirements for sampling rate. For low-frequency bands, as long as aliasing can be avoided, low sampling rate is actually preferable because it is then possible to capture data over a longer period of time.

To address this issue, one solution is to divide the frequency range of interest into several bands. For example, if the desired frequency range is from 0.1 Hz to 1 kHz, four frequency bands can be considered: 0.1 Hz to 1 Hz, 1 Hz to 10 Hz, 10 Hz to 100 Hz, and 100 Hz to 1 kHz. In this case, one injection is needed for each decade, and the random PWM signal is designed to have the maximum energy at the center of the band. Four RNNs, each corresponding to a frequency band, are then used to process the four sets of recorded data. The identified impedance information can then be combined to be used for stability analysis. Although this approach is more complicated than the single-injection method, it can significantly reduce the training time of the RNNs. Compared with conventional methods, the number of injections it requires is still much lower.

Fig. 13 illustrates the training process of the RNN network for frequency band 1 Hz to 10 Hz. It can be seen that the mean squared error (MSE) decreases rapidly during the initial several epochs. The reduction in MSE gradually slows down as the number of epochs increases. After about 20 iterations, the MSE settles down at a value slightly lower than 0.01. It is important to note that this value is much larger than those in simulation tests, which can be as low as 10^{-6}. The main reason for the discrepancy is that the experimental data contain much more noises, which have a negative impact on the RNN training process.

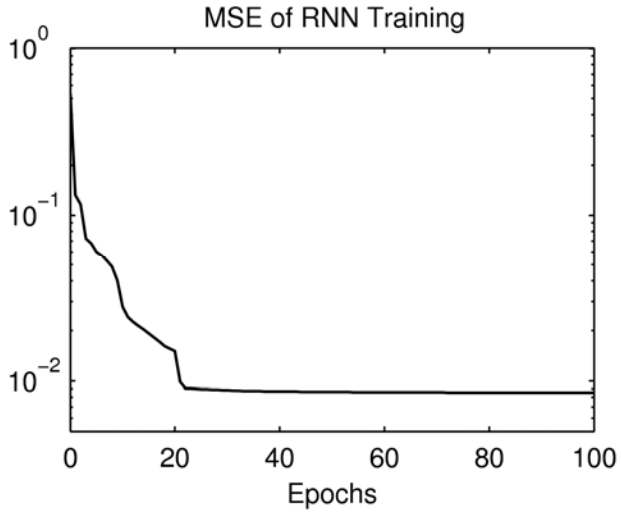

Fig. 13. Mean squared error of RNN during the training process.

When the training is finished, the outputs of the RNN are compared with the measured data. The comparison is depicted in Fig. 14, where the top trace shows the data recorded from the system, and the bottom trace represents the RNN outputs. It can be clearly seen that there is a very good agreement between the two, which indicates that the trained RNN is an accurate model of the system under test. It is worth mentioning that the measured data are normalized before the training.

Fig. 15 shows the comparison between the actual dc load impedance and the values identified based on the trained RNNss, where the top traces represent the magnitudes, and the bottom traces represent the phase angles. The effectiveness of the proposed method is confirmed by the apparent agreement between the two traces. It should be noted that at higher frequencies, noises in the sampled data make the training difficult to converge and thus degrade the accuracy of the method.

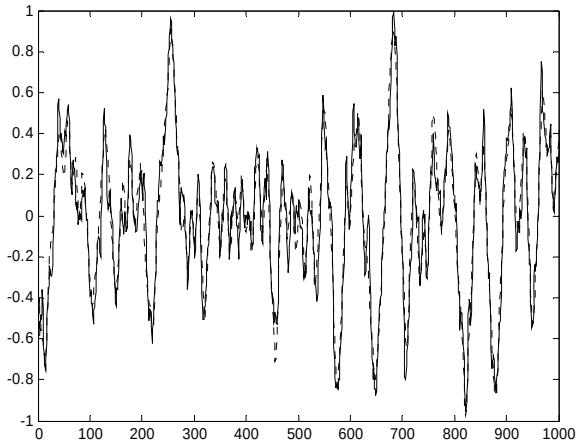

Fig. 14. Comparison between the measured (solid line) and RNN-estimated (dashed line) normalized currents.

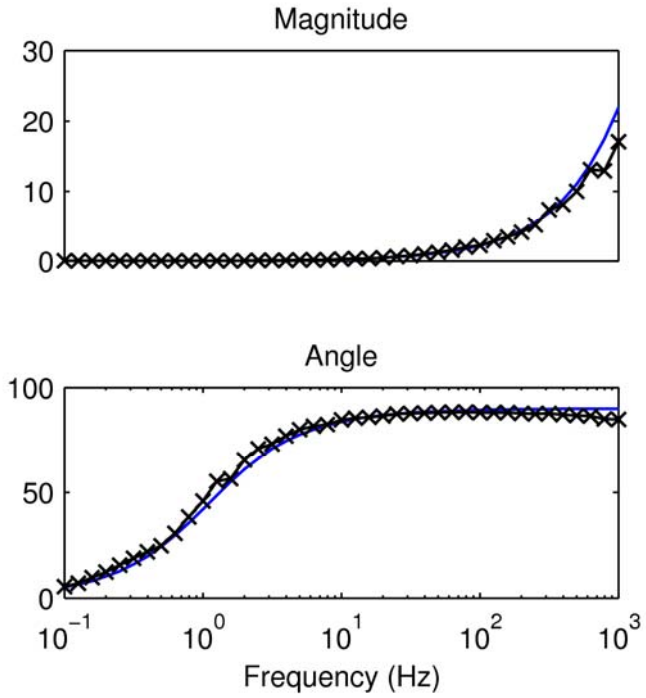

Fig. 15. Comparison between the actual and identified admittances.

6. CONCLUSIONS

By modeling the small-signal dynamics of a power electronic system with recurrent neural networks, the proposed impedance identification method significantly

reduces the online test time to extract the frequency-dependent impedance characteristics, which provide vital information for stability analysis. Random PWM signals and resistive chopper circuits are used to inject perturbation signals into the system under test, which produces voltage and current signals for RNN training. Both simulation and laboratory tests have been used to verify the effectiveness of the proposed method.

7. REFERENCES

[1] A. Emadi, A. Khaligh, C. H. Rivetta, et al., "Constant power loads and negative impedance instability in automotive systems: definition, modeling, stability, and control of power electronic converters and motor drives," *IEEE Transactions on Vehicular Technology*, vol. 55, pp. 1112-1125, Jul. 2006.

[2] R. D. Middlebrook, "Input filter considerations in design and application of switching regulators," *IEEE Proceedings of IASAM*, Oct. 1976.

[3] C. M. Wildrick, F. C. Lee, B. H. Cho, et al., "A method of defining the load impedance specification for a stable distributed power system," *IEEE Transactions on Power Electronics*, vol. 10, pp. 280-285, May 1995.

[4] S. D. Sudhoff, S. F. Glover, P. T. Lamm, et al., "Admittance space stability analysis of power electronic systems," *IEEE Transactions on* Aerospace *and Electronic Systems*, vol. 36, Part 1, pp. 965-973, Jul. 2000.

[5] Y. L. Familiant, K. A. Corzine, J. Huang, et al., "AC Impedance Measurement Techniques," *IEEE International Conference on Electric Machines and Drives*, pp.1850-1857, May 2005.

[6] M. Belkhayat and M.L. Williams, "Impedance Extraction Techniques for Dc and Ac Systems," *Proceedings of the Naval Symposium on Electric Machines*, Philadelphia PA, Dec. 2000.

[7] J. Huang and K. A. Corzine, "AC Impedance Measurement by Line-to-Line Injected Current," *Proceedings of IEEE IAS Annual Conference*, Oct. 2006.

[8] T. G. Barbounis, J. B. Theocharis, et al., "Long-term wind speed and power forecasting using local recurrent neural network models," *IEEE Transactions on Energy Conversion*, vol. 21, pp. 273-284, Mar. 2006.

[9] C. J. Chen and T. C. Chen, "Design of a Power System Stabilizer Using a new Recurrent Neural Network," *Innovative Computing, Information and Control*, *ICICIC '06*., vol. 1, pp. 39-43, Aug. 2006.

[10] A. Goedtel, I. N. daSilva, and P. J. Amaral Serni, "Recurrent Neural Network for Induction Motor Speed Estimation in Industry Applications," *IEEE MELECON*, pp. 1134-1137, Aug. 2006.

[11] P. Palangpour, G. K. Venayagamoorthy. and K. Duffy, "Recurrent Neural Network Based Predictions of Elephant Migration in a South African Game Reserve," *International Joint Conference on Neural Networks*, pp. 4084-4088, Jul. 2006.

[12] Y. D. Valle, G. K. Venayagamoorthy, S. Mohagheghi, et al., "Particle Swarm Optimization: Basic Concepts, Variants and Applications in Power Systems," *IEEE Transactions on Evolutionary Computation*, in press.

VITA

Peng Xiao was born in Henan, China on January 18, 1976. He received his Bachelor's degree in Electrical Engineering from Chongqing University in China in July, 1997. In April, 2000, he obtained his Master of Science degree in Electrical Engineering from North China Electric Power University, Beijing, China. He came to the United States in 2002 to further pursue his interest in the areas of power engineering and received an MS degree in Electrical Engineering from the University of Wisconsin-Milwaukee in August 2004. He then studied at the University of Missouri-Rolla and earned his Ph.D. degree in Electrical Engineering in December 2007.